



NTNU – Trondheim
Norwegian University of
Science and Technology

Development and Commissioning of a DP system for ROV SF 30k

Viktor Berg

Marine Technology
Submission date: June 2012
Supervisor: Asgeir Johan Sørensen, IMT

Norwegian University of Science and Technology
Department of Marine Technology



NTNU

Norwegian University of Science and Technology

MASTER THESIS

SPRING 2012

Development and Commissioning of a DP system for ROV SF 30k

Keywords: Vessel modelling,

Co-advisors:

Fredrik DUKAN

Martin LUDVIGSEN

Supervisor:

Prof. Asgeir SØRENSEN

Author:
Viktor BERG

June 8, 2012



MASTER THESIS IN MARINE CYBERNETICS

SPRING 2012

STUD. TECHN. VIKTOR BERG

Development and Commissioning of a DP system for ROV SF 30k

Work description:

At NTNU AUR-Lab, a dynamic positioning (DP) system is developed for the ROV Minerva. AUR-Lab does also operate a second ROV, SF 30k. In this MSc thesis the development and commissioning of DP system for the ROV SF 30k will be addressed.

This includes adaptation of software architecture and code, the modification and brief tuning of control parameters, including the Kalman observer, the DP controller(s), the thrust allocation system and the vehicle interface system (input/output) to sensors and thrusters. The scope of the thesis requires extensive modification of large parts of the system in the existing DP system done together with researchers and other MSc students. A sea trial is planned to document the work done.

Scope of work:

1. Review of documentation of DP system for ROV Minerva, and specifications of ROV SF 30k.
2. Modelling and determination of the parameters and coefficients for ROV SF 30k by hydrodynamic SW code, and experience from ROV Minerva.
3. Modification of the LabView structure of the DP system.
4. Brief tuning and adjustments of the system based on sea trials.
5. Carrying out sea trials and documenting the results.

The report shall be written in English and edited as a research report including literature survey, description of mathematical models, description of control algorithms, simulation results, model test results, discussion and a conclusion including a proposal for further work. Source code should be provided on a CD with code listing enclosed in appendix. It is supposed that Department of Marine Technology, NTNU, can use the results freely in its research work, unless otherwise agreed upon, by referring to the student's work. The thesis should be submitted in three copies within June 10th.

Advisors: Dr. Martin Ludvigsen and PhD candidate Fredrik Dukan

Professor Asgeir J. Sørensen
Supervisor

Preface

The work within this thesis was done within the time span of the Spring 2012 semester, as a part of the Applied Underwater Robotics Laboratory at the Norwegian University of Science and Technology (NTNU). The main motivation of the thesis was the delivery of a working control system for the ROV SF 30k.

This thesis was a part of a larger project of designing and developing a new DP system for NTNU-owned ROVs during Spring 2012. A part of this work was thus written in collaboration with Espen Tolpinrud. This includes Chapter 4 (Section 4.1) and Chapter 5.

Abstract

This Master thesis details the development of a mathematical model of ROV SF 30k, and its implementation into a DP control system developed by Espen Tolpinrud. The project was performed as a part of the Applied Underwater Robotics at NTNU.

A 6DOF model of the ROV was developed. The parameters of the model were found using both the 3D model of the ROV provided by Sperre AS, and based on the parameters found previously for ROV Minerva. Both ROVs were developed by Sperre AS and share many similarities. Thrust configuration was developed for the ROV based on the geometric positions and orientations of its thrusters, while thrust coefficients were found using propeller data provided by Sperre AS. The DP control system was configured to operate SF 30k by using a configuration file based on the found parameters.

A number of modules were ported from the old DP system, which was tailor-made for ROV Minerva, to the new one. This includes the Kalman Filter, controllers and thrust allocation. An adaptive passive nonlinear observer was developed and implemented.

The existing simulator model for ROV Minerva was modified to be able to simulate ROV SF 30k. This was done by changing the parameters of the process plant model and thrust dynamics.

The parameters in the configuration file for the new control system were verified during sea trials onboard R/V Gunnerus on May 29-30th 2012. The thrust allocation parameters were found to be satisfactory during ROV operation, however, the mathematical model of the ROV could not be verified due to the small window of operation during the sea trials.

Acknowledgments

This project is a result of collaboration between several students within the AUR-Lab, both Master and PhD. I have worked alongside brilliant minds, and this thesis would not have been possible without their assistance and help.

First and foremost, I would like to thank my supervisor, Professor Asgeir Sørensen. During the course of writing this thesis, he provided me with a great amount of help and feedback on my progress, providing me with ideas for improvement and additions. At the same time, he did not restrict me in any way, and allowed me to approach the problems that I faced at my own pace.

I would also like to thank my co-advisors, PhD candidate Fredrik Dukan and Dr. Martin Ludvigsen. Fredrik helped me immensely when approaching the problems of working with the DP control system, as well as when developing the model for ROV SF 30k. Preparing the ROV for sea trials took a large amount of effort, and much of it was exerted by Fredrik. He also set up most of the telecommunication buffer system, which my work was based on. Martin Ludvigsen was an invaluable help in producing information on the SF 30k. Most of the information in the appendices of this thesis was provided by him, including the 3D model and specifications of the ROV.

Much of the work in this thesis was done in collaboration with Master candidate Espen Tolpinrud. The sheer amount of work he put into developing a flexible and powerful DP control system eased my work greatly. Due to the fact that we sat in the same office, we could maintain contact throughout the day, which both motivated me and brightened my day, even in the dark winter months. In that context, I would also like to thank Mats Nåvik Hval who, along with Espen, kept me company in the long days of working on the thesis. He was also an immense help with many technical questions regarding the thesis.

Finally, in regards to the sea trials, I have to offer my sincere gratitude to the crew of R/V Gunnerus who made it possible. Their hospitality made the days of staying onboard the ship enjoyable and peaceful.

Nomenclature

η	Position vector
ν	Velocity vector
τ	Control force vector
τ_{cable}	Umbilical force vector
η_d	Desired position
η_{ref}	Position reference
$\hat{\eta}$	Estimated position
I_b	Inertia matrix
$I_{n \times n}$	Identity matrix of size $n \times n$
K	Thrust coefficient matrix
$T(\alpha)$	Thrust configuration matrix
χ	Number of flop per cycle on a given processor
∇	Volume displacement
ω	Frequency
ρ	Water density
σ_{flop}	Number of flop per iteration
ϖ	data size in byte
C	Coriolis and centripetal matrix
C_D	Drag coefficient
D_L	Linear damping matrix
D_{NL}	Nonlinear damping matrix

f_{core}	Clock Frequency for a given processor
$flop$	FLoating-point OPeration
$flops$	Floating-point Operations Per Second
g	Gravitational constant
J	Transformation matrix
M	Mass matrix
M_A	Added mass matrix
M_{RB}	Rigid body mass matrix
N	Number of elements to be stored
n_{core}	Number of cores
n_{iter}	Number of iterations
AHRS	Attitude and Heading Reference System
AUR-Lab	Applied Underwater Robotics Laboratory
AUV	Autonomous Underwater Vehicle
BODY	Body-fixed
CB	Center of Buoyancy
CG	Center of Gravity
CO	Center of Origin
DOF	Degree Of Freedom
DP	Dynamic Positioning
HIL	Hardware In the Loop
HPR	Hydroacoustic Position Reference
LQR	Linear-Quadratic Regulator
MRU	Motion Reference Unit
N	Newton
NED	North East Down
NED	North-East-Down
NTNU	Norwegian University of Science and Technology

PID	Proportional-Integral-Derivative
R/V	Research Vessel
ROV	Remotely Operated Vehicle
RPM	Rotations Per Minute
SIL	Software In the Loop
Telebuf	Telecommunication buffer
UUV	Unmanned Underwater Vehicle
WF	Wave frequency

Contents

1	Introduction	3
1.1	Underwater Vehicles	3
1.2	Unmanned Underwater Vehicles	3
1.2.1	Autonomous Underwater Vehicles	4
1.2.2	Remotely Operated Vehicles	4
1.3	Applied Underwater Robotics Lab	5
1.4	ROV Minerva	5
1.5	ROV SF 30k	5
1.6	Control systems for marine vessels	7
1.7	Vessel modelling	8
1.8	Contributions	9
1.9	Outline of thesis	9
2	Vessel modelling	11
2.1	Kinematics	11
2.2	Kinetics	13
2.2.1	Rigid body kinetics	13
2.2.2	Hydrostatics	14
2.2.3	Hydrodynamics	14
2.2.4	Damping	15
2.3	Umbilical forces	17
2.4	Control forces	18
3	Modelling of ROV SF 30k	21
3.1	Vessel model	21
3.1.1	Mass and added mass calculations	22
3.1.2	Damping	28
3.1.3	Restoring forces and moments	31
3.1.4	Umbilical forces	31
3.2	Thrust allocation	32
3.2.1	Thrust configuration matrix	32
3.2.2	Thrust coefficient matrix	37
3.2.3	Thrust loss	39

4 Control system	41
4.1 6DOF adaptation	41
4.1.1 Observers	41
4.1.2 Guidance systems	45
4.1.3 Controllers	47
4.1.4 Thrust allocation	48
4.2 SF 30k telecommunication implementation	48
4.3 SIL and HIL simulator models	49
5 Commissioning and sea trials	51
6 Conclusions and further work	57
6.1 Conclusions	57
6.2 Recommendations for further work	58
A ROV 30k specifications	I
B Model files	VII
B.A Original model	VII
B.B Simplified model	VII
B.C Converted model	VII
B.D WAMIT model	VII
B.E Model used to calcualte projected area	VII
C RPM-to-thrust data	IX
D Information on the telecommunication buffer for ROV SF 30k	XIII

List of Figures

1.1	ROV Minerva (from [9]).	6
1.2	ROV SF 30k mid-emergence while being lifted by R/V Gunnerus. . .	7
1.3	The real-time control structure, taken from [12].	8
2.1	The setup of the umbilical cable, with the vertical tangent point shown.	18
3.1	Original AutoCAD model with added weight emulating sensory systems.	23
3.2	Simplified model intended for WAMIT analysis.	24
3.3	ROV thruster positions, top view.	33
3.4	ROV thruster positions, side view.	34
3.5	ROV thruster positions, front view.	34
3.6	ROV thruster IDs.	35
3.7	The regressed thrust-RPM curve and the fitted coefficient.	38
4.1	Complete model of the adaptive nonlinear passive observer.	45
4.2	Wave filter subsystem including adaptive law.	46
4.3	Modified bias estimator.	46
4.4	Modified wave estimator.	47
4.5	The basic concept of hardware-in-the-loop simulation (from [33]). . .	50
5.1	Plots of Translational motion during DP test.	52
5.2	Plots of Rotational motion during DP test.	53
5.3	Plots of Translational motion during Direct Thrust Allocation Mode with Joystick.	54
5.4	Plots of Rotational motion during Direct Thrust Allocation Mode with Joystick.	55

Chapter 1

Introduction

The aim of this thesis is to commission the Dynamic Positioning system (DP system) outlined in Master's thesis by Espen Tolpinrud [1] for ROV SF 30k. This project is a part of the Applied Underwater Robotics Laboratory (AUR-Lab), which is a collaboration between the different faculties within the Norwegian University of Science and Technology (NTNU). An effort is being made into procuring additional assets for the operations, which includes putting ROV SF 30k into operation. The goal of this thesis is to provide the ability to use the DP system on SF 30k, thus including it as an active asset for AUR-Lab.

1.1 Underwater Vehicles

According to [2], an underwater vehicle is defined as: “a small vehicle that is capable of propelling itself beneath the water surface as well as on the water surface. This includes unmanned underwater vehicles (UUV), remotely operated vehicles (ROV), autonomous underwater vehicles (AUV) and underwater robotic vehicles (URV)”. Underwater vehicles are a relatively new addition to the list of man-made seafaring vehicles. The first such vehicles were submarines, the first of which was built in 1620 by Cornelius Jacobszoon Drebbel using design standards outlined by William Bourne [3]. Their significance within the military field was quickly recognized, and in 1775, the first military submarine, “Turtle”, was built by David Bushnell [4].

1.2 Unmanned Underwater Vehicles

Unmanned underwater vehicles describe all vehicles that can operate underwater without a human operator in them. They are typically divided into two categories: AUVs and ROVs. The earliest application of UUVs, also sometimes called underwater drones, were torpedoes. Later on, UUVs were taken into use in a wide variety of non-military fields, most particularly the oil & gas industry, since the use of UUVs significantly simplifies deep sea operations [5].

1.2.1 Autonomous Underwater Vehicles

The Autonomous Underwater Vehicle is a device that can operate underwater without any connection to the surface, with all the systems installed onboard, including a power supply [6]. Such a configuration greatly improves the flexibility of such a vehicle, since it is not bound by constraints to a point in the sea, and can operate over longer distances, and in more complex environments. However, development and usage of AUVs provides additional challenges. An AUV must be able to host a power source with sufficiently high capacity to perform long duration operations. Additionally, the operating system of an AUV must be sophisticated enough to ensure completely autonomous operation. AUVs are most often shaped to have minimal damping and to maximize battery life, and are often underactuated, which is to say, it is not possible to control every DOF (degree of freedom) individually.

1.2.2 Remotely Operated Vehicles

In contrast to AUVs, Remotely Operated Vehicles are underwater vehicles that are connected to the operator on the surface by a umbilical cable. There is also less concern as to the shape of the ROV, since the power to the vehicle is provided through the umbilical cable, and thus the only concern is maximum movement speed. Since the ROV is controlled by a human operator, it is often equipped with a wide assortment of tools, cameras and lights, which makes it possible to perform a wide variety of tasks. ROVs are also fully actuated, and are thus better suited than AUVs to performing tasks that require high precision.

ROVs are typically classified into different categories [7]. An example of classification is shown in the table below.

- Micro - very small ROVs. Typical weight is within 2-10kg. Mainly used as a means to access places that a human diver cannot enter. Can only perform surveillance tasks.
- Mini - somewhat larger than the Micro category, typical weight is around 15kg. Serves a similar role to the Micro. It is also mainly used for surveillance, which is why this class (as well as the Micro class) are sometimes called the “eyeball” classes.
- General - the smallest class of ROVs that can perform intervention tasks. They have typically less than 5 horsepower (HP) (3750 Watts) propulsion, and have an operating depth of less than 1000m on average. Manipulators are sometimes installed on general class ROVs.
- Light Workclass - less than 50HP (37.5kW) propulsion. Usually fitted with one or several manipulators. Working depth of less than 2000m.
- Heavy Workclass - less than 220HP (165kW) propulsion. Carry at least 2 manipulators. Working depths of up to 3500m.
- Trenching/Burial - between 200-500HP (150-375kW) propulsion. Equipped with a cable laying sled, and able to operate at depths of up to 6000m.

1.3 Applied Underwater Robotics Lab

The Applied Underwater Robotics Laboratory (AUR-Lab) was established by NTNU in late 2009. Its purpose is to provide an ability to join the efforts of experts from cybernetics, control engineering, marine biology, marine archaeology, electrical engineering and communications. The result is a joint effort in research and development in the field of underwater robotics [8]. As of June 2012, the AUR Lab has two ROVs: ROV Minerva and ROV SF 30k, with the latter being a recent addition. The ROV operations are performed onboard R/V Gunnerus approximately once a month. There are also plans of acquiring an AUV.

1.4 ROV Minerva

ROV Minerva was designed and produced by Sperre AS for NTNU in 2003. The base model for Minerva is called the SUB-Fighter 7500. It is used for biological research and sampling, as well as development of new control technology, archaeological and geological surveys etc. Minerva has the dimensions of 1.44m long, 0.82m wide and 0.8m high, and weighs 450kg [16]. It is equipped with 5 2HP thrusters (1.5kW), each providing between 300-340N thrust force. Two of the thrusters are vertical, two thrusters provide forward and backward thrust, and the last one is a tunnel thruster providing lateral thrust. The two vertical thrusters are positioned on the left and the right sides of the ROV, but are combined to have the same shaft speed in the control system. This makes the ROV underactuated in roll. However, due to the position of the thrusters, it would be impossible to control pitch independently even if it was possible to control the thrusters individually. The ROV carries a manipulator without position feedback, a sonar, 4 lights, 4 cameras and a range of sensors measuring depth and heading. The umbilical connecting the ROV to the winch is 600m long. According to the classification outlined in Section 1.2.2 ROV Minerva can be classified as a general class ROV. Figure 1.1 shows ROV Minerva [9].

1.5 ROV SF 30k

ROV SUB-Figher 30000 (also called SF 30k), just like ROV Minerva, was produced by Sperre AS. A working name “Neptune” was proposed by Fredrik Dukan, but was not finalized at the time of writing this thesis. The ROV was used by Trondheim Biological Station until December 2010. It has a length of 2.5m, a width of 1.5m, a height of 1.6m and has a weight of 1850kg (Appendix A). There are 6 thrusters with 3kW installed on the ROV, with a similar thruster configuration to that of ROV Minerva, with the addition of a third vertical thruster. This ROV is also underactuated in pitch and roll, since the 3 vertical thrusters are given the same RPM by the control box and are impossible to control independently of one another. A “Raptor” model manipulator was installed onto the ROV [10]. Other equipment includes 4 cameras, 4 lights, as well as a wide range of sensors including:



Figure 1.1: ROV Minerva (from [9]).

- Sonar
- Multibeam
- Cable tracker
- Side scan
- Altimeter
- Doppler log
- Motion reference unit (MRU)
- Lasers
- Hydroacoustic position reference system (HPR)

The SF 30k is connected to the winch with a 1100m long umbilical cable, almost double that of Minerva's cable length. The maximum listed working depth for ROV SF 30k is 3000m, which is constrained by the umbilical. Due to these specifications, SF 30k can be placed between general class and light worker class ROVs in the classification table. Figure 1.2 shows the ROV being lifted from water by R/V Gunnerus during sea trials on May 30th.



Figure 1.2: ROV SF 30k mid-emergence while being lifted by R/V Gunnerus.

1.6 Control systems for marine vessels

The development of automated control systems for ships started as early as late 19th century [11]. They started off as simple PI controllers operating as binary switches, turning the actuators on or off based on the error. However, in 1939, a controller with continuously variable control action was introduced. This allowed smooth control without the inevitable chattering produced by the binary nature of early controllers. One of the first marine vessels to make use of automated control was the U.S. battleship “New Mexico”. During the period of the early 20th century, great strides were made in the control theory, as military vessels required movement compensating systems in order to increase the precision of artillery fire.

The real-time control system structure (taken from [12]) is outlined in Figure 1.3. Every layer from the bottom up increases the level of control in the real-time system.

- *Actuator control* - performs local control on the actuators present on the vessel: propellers, rudders, azimuth thrusters, etc. The control may be exerted upon the speed, torque or thrust of the actuators, or else a combination of them.
- *Plant control* - this layer calculates the controlling forces based on input signals, including wind, wave and current loads, as well as position and velocity measurements. This layer typically houses observers (which estimate system states to account for events like dead reckoning and non-measured data, as

well as with the purpose of wave filtering), controllers (which employ a control algorithm to calculate the control forces based on position and velocity input) and thrust allocation (which distributes thrust setpoints to the actuators based on the control vector and the actuator configuration on the vessel).

- *Local optimization* - provides an optimized set of instructions to the plant control based on the current task at hand. This layer houses systems that are responsible for generating movement trajectories and position setpoints. This includes tracking and guidance systems, as well as DP mode controls.

The focus of this thesis lies mainly within the plant control layer of the control structure.

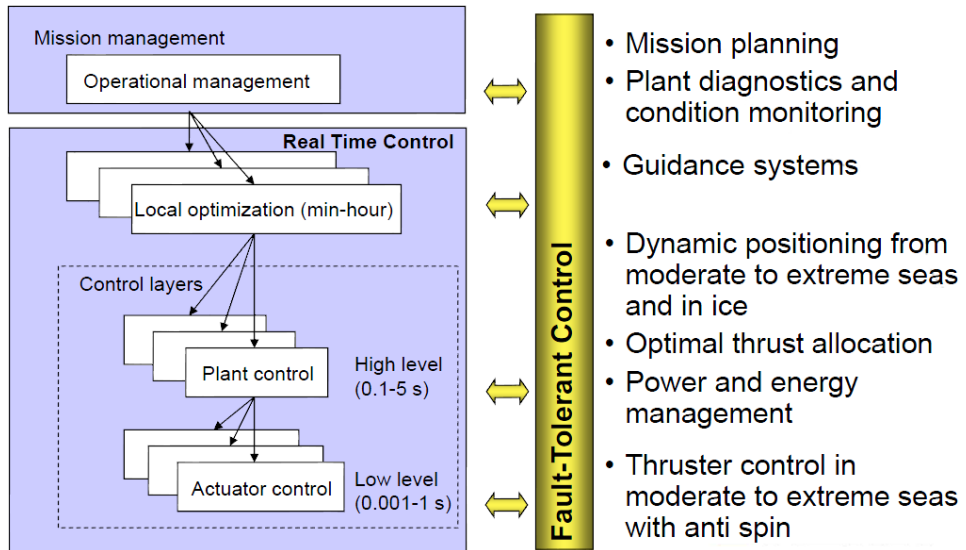


Figure 1.3: The real-time control structure, taken from [12].

1.7 Vessel modelling

Several stages of development of an efficient control system require a reasonably accurate model of the controlled vessel. This includes observers, certain control algorithms and thrust allocation. Additionally, in order to develop a simulator of the system, the model parameters have to be calculated or estimated as accurately as possible, often more accurately than the model developed for a control system.

Vessel modelling is performed using various techniques, both analytical, numeric and empirical. In many cases, an analytic solution is not possible, or is too computationally heavy, in which case an approximate solution might be found using

either computer-based numeric methods, or tests performed either on a scaled down model, or in full scale if possible.

1.8 Contributions

The contributions of the author of this thesis are outlined in this section. These include:

- A mathematical model describing ROV SF 30k has been developed in Chapter 3. The parameters for inertial, damping and restoring forces have been calculated either analytically, numerically or estimated based on ROV Minerva.
- The model was implemented into the DP control system developed by Espen Tolpinrud [1], into the configuration file describing the ROV. This includes the data for establishing the observers, the controllers and the thrust allocation system.
- A number of modules were adapted from the old DP system, which was developed exclusively for ROV SF 30k, into the new DP system. These modules were reworked to be more generalized, and thus work on any ROV provided the correct configuration file is provided. These modules include the Kalman Filter, the four controllers (linear and nonlinear PID, LQR, sliding mode). This process is outlined in Chapter 4.
- An adaptive nonlinear passive observer has been developed and implemented into the control system (also shown in Chapter 4).
- The original HIL/SIL simulators used for testing ROV Minerva have been partially reworked to be able to simulate ROV SF 30k. This includes the adjusted vessel model, thrust dynamics and telecommunication buffer implementation. In addition, the simulators were modified to be more flexible and accept additional ROVs.

1.9 Outline of thesis

Chapter 2 presents theory on modelling of vessel parameters, mostly based on [2]. The result is a vessel process plant model in 6DOF.

Chapter 3 presents the process and results of estimating model parameter values. The methods used vary from analytical to numerical to empirical (based on ROV Minerva). The numerical methods include using SolidWorks, Rhinoceros and WAMITv6. In addition a thrust allocation system is set up for the ROV.

Chapter 4 outlines the work done on the ROV DP control system in collaboration with Espen Tolpinrud. In particular the development of the adaptive

nonlinear passive observer is presented, as well as the modification of the SIL and HIL simulators.

Chapter 5 shows the results of ROV behavior when controlled by the DP control system using the model parameters found in Chapter 3. The validity of the thrust allocation algorithm is tested, and preliminary tuning of the observer is performed.

Appendix A contains the specifications of ROV SF 30k.

Appendix B contains all the 3D models that were used during the calculation or estimation of parameters in Chapter 3.

Appendix C contains graphs that detail thruster characteristics for ROV SF 30k.

Appendix D contains information about the telecommunication buffer for the ROV. This document was written by Fredrik Dukan.

Chapter 2

Vessel modelling

The goal of this chapter is to establish a mathematical model of an ROV. Since the control system which will use this model will operate in real time, a relatively simple control plant model has to be used. Still, the information on various values has to be as accurate as possible. However, due to the unavailability of some of the required information, assumptions have to be made on a number of occasions.

The ROV is to be used mostly outside of the wave-zone, and as such, the control plant is not required to simulate wave forces and motions. As well, due to the low velocity of the ROV, a high amount of coupling is expected in most terms, including the inertial forces, Coriolis-centripetal forces and damping forces.

The ROV will be modelled using the general equations of motion for a marine craft, which can be expressed in vectorial form according to [13]:

$$\dot{\boldsymbol{\eta}} = \mathbf{J}_\Theta(\boldsymbol{\eta})\boldsymbol{\nu} \quad (2.1)$$

$$\mathbf{M}\dot{\boldsymbol{\nu}} + \mathbf{C}(\boldsymbol{\nu})\boldsymbol{\nu} + \mathbf{D}(\boldsymbol{\nu})\boldsymbol{\nu} + \mathbf{g}(\boldsymbol{\eta}) = \boldsymbol{\tau} + \boldsymbol{\tau}_{cable} \quad (2.2)$$

The vectors $\boldsymbol{\eta}$ and $\boldsymbol{\nu}$ are the vessel's position and velocity vectors respectively. $\boldsymbol{\tau}$ is the control force vector, and $\boldsymbol{\tau}_{cable}$ is the vector describing the umbilical forces from the cable attached to the ROV.

2.1 Kinematics

The ROV SF 30k is stable in roll and pitch, which means that typically, a 4DOF model would suffice. However, since the secondary objective of this project is to make the DP system more flexible for use on any arbitrary ROV, the system will be modified for 6DOF.

- The Earth-fixed frame (**NED**) is a reference frame that is usually defined as the tangent plane on the surface of the Earth moving with the craft. For this reference frame, the x -axis points towards *North*, the y -axis points towards *East*, and the z -axis points *Down*. Considering that the motions of the ROV are rather small in scale, the NED frame can be considered inertial.

- The body-fixed frame (**BODY**) is a moving reference frame that is fixed to the craft. Its axes coincide with the principal axes of inertia, where the x -axis is longitudinal (directed from aft to fore), the y -axis is transversal (directed to starboard), and z -axis is normal (directed from top to bottom).

Typically, a vessel's position and orientation are expressed in NED, while its linear and angular velocities are expressed in BODY. These values are expressed using the SNAME notation [14], which is given in Table 2.1.

Table 2.1: SNAME notation.

DOF	Description	Forces	Velocities	Positions
1	Surge	X	u	x
2	Sway	Y	v	y
3	Heave	Z	w	z
4	Roll	K	p	ϕ
5	Pitch	L	q	θ
6	Yaw	M	r	ψ

According to [2], motions of a vessel can be described as following vectors:

$$\boldsymbol{\eta} = \begin{bmatrix} \mathbf{p}_{b/n}^n \\ \boldsymbol{\Theta}_{nb} \end{bmatrix}, \boldsymbol{\nu} = \begin{bmatrix} \mathbf{v}_{b/n}^b \\ \mathbf{w}_{b/n}^b \end{bmatrix}, \boldsymbol{\tau} = \begin{bmatrix} \mathbf{f}_b^b \\ \mathbf{m}_b^b \end{bmatrix} \quad (2.3)$$

Where:

- $\mathbf{p}_{b/n}^n = [x \ y \ z]^\top \in \mathbb{R}^3$ is NED position,
- $\boldsymbol{\Theta}_{nb} = [\phi \ \theta \ \psi]^\top \in \mathcal{S}^3$ is attitude in Euler angles,
- $\mathbf{v}_{b/n}^b = [u \ v \ w]^\top \in \mathbb{R}^3$ is BODY linear velocity,
- $\mathbf{w}_{b/n}^b = [p \ q \ r]^\top \in \mathbb{R}^3$ is BODY angular velocity,
- $\mathbf{f}_b^b = [X \ Y \ Z]^\top \in \mathbb{R}^3$ are body-fixed forces,
- $\mathbf{m}_b^b = [K \ M \ N]^\top \in \mathbb{R}^3$ are body-fixed moments.

The transformation between BODY and NED is performed using the following formula:

$$\dot{\boldsymbol{\eta}} = \mathbf{J}_\Theta(\boldsymbol{\eta})\boldsymbol{\nu}, \quad (2.4)$$

where $\mathbf{J}_\Theta(\boldsymbol{\eta})$ is the BODY-to-NED transformation matrix given by:

$$\mathbf{J}_\Theta(\boldsymbol{\eta}) = \begin{bmatrix} \mathbf{R}_b^n(\boldsymbol{\Theta}_{nb}) & \mathbf{0}_{3 \times 3} \\ \mathbf{0}_{3 \times 3} & \mathbf{T}_\Theta(\boldsymbol{\Theta}_{nb}) \end{bmatrix}, \quad (2.5)$$

$\mathbf{R}_b^n(\Theta_{nb})$ and $\mathbf{T}_\Theta(\Theta_{nb})$ are given by:

$$\mathbf{R}_b^n(\Theta_{nb}) = \begin{bmatrix} c\psi c\theta & -s\psi c\phi + c\psi s\theta s\phi & s\psi s\phi + c\psi c\phi s\theta \\ s\psi c\theta & c\psi c\phi + s\phi s\theta s\psi & -c\psi s\phi + s\theta s\psi c\phi \\ -s\theta & c\theta s\phi & c\theta c\phi \end{bmatrix} \quad (2.6)$$

$$\mathbf{T}_b^n(\Theta_{nb}) = \begin{bmatrix} 1 & s\phi t\theta & c\phi t\theta \\ 0 & c\phi & -s\phi \\ 0 & \frac{s\phi}{c\theta} & \frac{c\phi}{c\theta} \end{bmatrix}, c\theta \neq 0 \rightarrow \theta \neq 90\text{degrees}, \quad (2.7)$$

where $c(\cdot) = \cos(\cdot)$, $s(\cdot) = \sin(\cdot)$ and $t(\cdot) = \tan(\cdot)$.

2.2 Kinetics

The motion of a marine craft can be divided into rigid body motions, hydrostatics and hydrodynamics.

2.2.1 Rigid body kinetics

According to [13], rigid body kinetics can be expressed as:

$$\mathbf{M}_{RB}\dot{\nu} + \mathbf{C}_{RB}(\nu)\nu = \tau_{RB} \quad (2.8)$$

Here, \mathbf{M}_{RB} is the rigid body mass matrix, \mathbf{C}_{RB} is the rigid body Coriolis and centripetal matrix due to the rotation of BODY about NED, and τ_{RB} is the generalized vector of external forces and moments expressed in BODY.

\mathbf{M}_{RB} is a matrix unique to the geometry of the body. It is symmetric, positive definite and constant, which means that it satisfies the following criteria:

$$\mathbf{M}_{RB} = \mathbf{M}_{RB}^\top > 0, \dot{\mathbf{M}}_{RB} = \mathbf{0}_{6 \times 6} \quad (2.9)$$

According to [2], \mathbf{M}_{RB} is defined as:

$$\begin{aligned} \mathbf{M}_{RB} &= \begin{bmatrix} m\mathbf{I}_{3 \times 3} & -m\mathbf{S}(\mathbf{r}_g^b) \\ m\mathbf{S}(\mathbf{r}_g^b) & \mathbf{I}_b \end{bmatrix} \\ &= \begin{bmatrix} m & 0 & 0 & 0 & mz_g & -my_g \\ 0 & m & 0 & -mz_g & 0 & mx_g \\ 0 & 0 & m & my_g & -mx_g & 0 \\ 0 & -mz_g & my_g & I_x & -I_{xy} & -I_{xz} \\ mz_g & 0 & -mx_g & -I_{yx} & I_y & -I_{yz} \\ -my_g & mx_g & 0 & -I_{zx} & -I_{zy} & I_z \end{bmatrix} \end{aligned} \quad (2.10)$$

Here, m is the mass of the vehicle, $\mathbf{I}_{3 \times 3}$ is the identity matrix, \mathbf{I}_b is the inertia matrix, and $\mathbf{S}(\mathbf{r}_g^b)$ is the skew-symmetric matrix, where \mathbf{r}_g^b is location of center of gravity (CG) with respect to center of origin (CO). $\mathbf{S}(\mathbf{r}_g^b)$ is defined as:

$$\mathbf{S}(\mathbf{r}_g^b) = \begin{bmatrix} 0 & -z_g & y_g \\ z_g & 0 & -x_g \\ -y_g & x_g & 0 \end{bmatrix}, \quad (2.11)$$

where $\mathbf{r}_g^b = [x_g \ y_g \ z_g]^\top$.

The Coriolis and centripetal matrix $\mathbf{C}_{RB}(\boldsymbol{\nu})$ can be defined in several ways. For the purposes of this paper, the Lagrangian parameterization is used, according to [15]:

$$\begin{aligned} & \mathbf{C}_{RB}(\boldsymbol{\nu}) \\ &= \begin{bmatrix} \mathbf{0}_{3 \times 3} & -m\mathbf{S}(\boldsymbol{\nu}_1) - m\mathbf{S}(\boldsymbol{\nu}_2)\mathbf{S}(\mathbf{r}_g^b) \\ -m\mathbf{S}(\boldsymbol{\nu}_1) + m\mathbf{S}(\mathbf{r}_g^b)\mathbf{S}(\boldsymbol{\nu}_2) & -\mathbf{S}(\mathbf{I}_b\boldsymbol{\nu}_2) \end{bmatrix} \end{aligned} \quad (2.12)$$

Here, $\boldsymbol{\nu}_1 = \mathbf{v}_{b/n}^b$, $\boldsymbol{\nu}_2 = \mathbf{w}_{b/n}^b$.

2.2.2 Hydrostatics

The hydrostatic vector $\mathbf{g}(\boldsymbol{\eta})$ will create restoring forces and moments and can, according to [2], be expressed as:

$$\mathbf{g}(\boldsymbol{\eta}) = \begin{bmatrix} (W - B)s(\theta) \\ -(W - B)c(\theta)s(\phi) \\ -(W - B)c(\theta)c(\phi) \\ -(y_g W - y_b B)c(\theta)c(\phi) + (z_g W - z_b B)c(\theta)s(\phi) \\ (z_g W - z_b B)s(\theta) + (x_g W - x_b B)c(\theta)c(\phi) \\ -(x_g W - x_b B)c(\theta)s(\phi) - (y_g W - y_b B)s(\theta) \end{bmatrix} \quad (2.13)$$

Here, $W = mg$ is the weight of the vehicle, $B = \rho_w g \nabla$ is the buoyant force, where g is the gravitational constant, ρ_w is the density of water, and ∇ is the volume displacement of the ROV. $\mathbf{r}_g^b = [x_g \ y_g \ z_g]^\top$ is the position of the its CG and $\mathbf{r}_b^b = [x_b \ y_b \ z_b]^\top$ is the position of its center of buoyancy (CB).

2.2.3 Hydrodynamics

According to [16], the hydrodynamic forces and moments on a body in 6DOF can be expressed as such:

$$\boldsymbol{\tau}_{hyd} = -\mathbf{M}_A \dot{\boldsymbol{\nu}}_r - \mathbf{C}_A(\boldsymbol{\nu}_r) \boldsymbol{\nu}_r - \mathbf{D}(\boldsymbol{\nu}_r) \boldsymbol{\nu}_r, \quad (2.14)$$

where $\mathbf{M}_A = \mathbf{M}_A^\top > 0 \in \mathbb{R}^{6 \times 6}$ is the added mass system inertia matrix, $\mathbf{C}_A = -\mathbf{C}_A^\top \in \mathbb{R}^{6 \times 6}$ is the hydrodynamic Coriolis-centripetal matrix and $\mathbf{D}(\boldsymbol{\nu}) \in \mathbb{R}^{6 \times 6}$ represents damping. $\boldsymbol{\nu}_r$ is the relative velocity of the body due to currents, expressed as: $\boldsymbol{\nu}_r = \boldsymbol{\nu} - \boldsymbol{\nu}_c$ where $\boldsymbol{\nu}_c = [u_c \ v_c \ w_c \ 0 \ 0 \ 0]^\top$. The current is assumed to be varying, thus $\dot{\boldsymbol{\nu}}_r = \dot{\boldsymbol{\nu}} - \dot{\boldsymbol{\nu}}_c$, where $\dot{\boldsymbol{\nu}}_c = [\dot{u}_c \ \dot{v}_c \ \dot{w}_c \ 0 \ 0 \ 0]^\top$.

Due to the ROV operating outside of the wave zone, the added mass matrix can be assumed approximately constant. It is defined according to [2] as following:

$$\mathbf{M}_A = \begin{bmatrix} \mathbf{A}_{11} & \mathbf{A}_{12} \\ \mathbf{A}_{21} & \mathbf{A}_{22} \end{bmatrix} = \begin{bmatrix} X_{\dot{u}} & X_{\dot{v}} & X_{\dot{w}} & X_{\dot{p}} & X_{\dot{q}} & X_{\dot{r}} \\ Y_{\dot{u}} & Y_{\dot{v}} & Y_{\dot{w}} & Y_{\dot{p}} & Y_{\dot{q}} & Y_{\dot{r}} \\ Z_{\dot{u}} & Z_{\dot{v}} & Z_{\dot{w}} & Z_{\dot{p}} & Z_{\dot{q}} & Z_{\dot{r}} \\ K_{\dot{u}} & K_{\dot{v}} & K_{\dot{w}} & K_{\dot{p}} & K_{\dot{q}} & K_{\dot{r}} \\ M_{\dot{u}} & M_{\dot{v}} & M_{\dot{w}} & M_{\dot{p}} & M_{\dot{q}} & M_{\dot{r}} \\ N_{\dot{u}} & X_{\dot{v}} & N_{\dot{w}} & N_{\dot{p}} & N_{\dot{q}} & N_{\dot{r}} \end{bmatrix} \quad (2.15)$$

Here, the SNAME notation [14] is used to determine the coefficients in the matrix. For instance $X_{\dot{w}}$ denotes the added mass force X along the x -axis due to fluid acceleration \dot{w} in the z -direction.

The hydrodynamic Coriolis and centripetal matrix can be defined as:

$$\mathbf{C}_A = \begin{bmatrix} \mathbf{0}_{3 \times 3} & -\mathbf{S}(\mathbf{A}_{11}\boldsymbol{\nu}_1 + \mathbf{A}_{12}\boldsymbol{\nu}_2) \\ -\mathbf{S}(\mathbf{A}_{11}\boldsymbol{\nu}_1 + \mathbf{A}_{12}\boldsymbol{\nu}_2) & -\mathbf{S}(\mathbf{A}_{21}\boldsymbol{\nu}_1 + \mathbf{A}_{22}\boldsymbol{\nu}_2) \end{bmatrix} \quad (2.16)$$

2.2.4 Damping

Hydrodynamic damping for marine craft has several different causes [2], such as:

1. **Potential damping:** caused by oscillation of a body with the wave excitation frequency in the absence of incident waves. It is worth noting that since ROV SF 30k operates outside of the wave-zone, this term will be omitted from the vessel model.
2. **Skin friction:** appears due to the friction between the surface of a moving body and the boundary layer of the fluid it moves in.
3. **Wave drift damping:** added resistance for surface bodies advancing in waves.
4. **Damping due to vortex shedding:** appears due to the shedding of vortices at sharp edges.

All of these damping terms can be rather difficult to separate from one another. In addition, for bodies that move in 6DOF, damping is highly nonlinear and coupled. However, it is common to divide damping into linear and nonlinear terms, as shown below:

$$\mathbf{D}(\boldsymbol{\nu}_r) = \mathbf{D}_L + \mathbf{D}_{NL}(\boldsymbol{\nu}_r) \quad (2.17)$$

\mathbf{D}_L are the linear, velocity-independent damping terms, while $\mathbf{D}_{NL}(\boldsymbol{\nu}_r)$ are the nonlinear terms that can change with the velocity of the body.

Nonlinear viscous damping

According to Fsn:11, the nonlinear damping matrix includes quadratic and higher order terms. It is typical to model this damping term using Morrison's equation as seen in [17]:

$$\mathbf{F}_D = \frac{1}{2} \rho C_D A_p |v| v, \quad (2.18)$$

where ρ is the density of the fluid, C_D is the drag coefficient, A_p is the projected area and v is the velocity of the body.

The drag coefficients can either be found empirically, or approximated based on previous tests performed on bodies of similar shape. In case of ROV SF 30k, it would be possible to approximate its drag coefficients to those of ROV Minerva, for which model-scale tests have been performed.

The full nonlinear uncoupled damping matrix becomes:

$$\mathbf{D}_{NL}(\boldsymbol{\nu}) = \frac{1}{2} \rho diag\{\mathbf{A}_p\} \quad (2.19)$$

$$diag\{C_{D,x}|u_r|, C_{D,y}|v_r|, C_{D,z}|w_r|, C_{D,\phi}|p_r|, C_{D,\theta}|q_r|, C_{D,\psi}|r_r|\}, \quad (2.20)$$

where bsA_p is the vector containing projected areas in all degrees of freedom.

Linear viscous damping

According to [2] the linear viscous damping matrix in CO with decoupled surge dynamics can be written as:

$$\mathbf{D}_L = \mathbf{D}_P + \mathbf{D}_V = - \begin{bmatrix} X_u & 0 & 0 & 0 & 0 & 0 \\ 0 & Y_v & 0 & Y_p & 0 & Y_r \\ 0 & 0 & Z_w & 0 & Z_q & 0 \\ 0 & K_v & 0 & K_p & 0 & K_r \\ 0 & 0 & M_w & 0 & M_q & 0 \\ 0 & N_v & 0 & N_p & 0 & N_r \end{bmatrix} \quad (2.21)$$

The diagonal terms can be expressed using seakeeping theory:

$$-X_u = B_{11v} \quad (2.22)$$

$$-Y_v = B_{22v} \quad (2.23)$$

$$-Z_w = B_{33v} + B_{33}(\omega_{heave}) \quad (2.24)$$

$$-K_p = B_{44v} + B_{44}(\omega_{roll}) \quad (2.25)$$

$$-M_q = B_{55v} + B_{55}(\omega_{pitch}) \quad (2.26)$$

$$-N_r = B_{66v} \quad (2.27)$$

Here, the B-terms can be calculated based on the system time constants T_{surge} , T_{sway} and T_{yaw} using the following formulas:

$$B_{11v} = \frac{m + X_u(0)}{T_{surge}} \quad (2.28)$$

$$B_{22v} = \frac{m + Y_v(0)}{T_{sway}} \quad (2.29)$$

$$B_{33v} = 2\Delta\zeta_{heave}\omega_{heave}[m + Z_w(\omega_{heave})] \quad (2.30)$$

$$B_{44v} = 2\Delta\zeta_{roll}\omega_{roll}[I_x + K_p(\omega_{roll})] \quad (2.31)$$

$$B_{55v} = 2\Delta\zeta_{pitch}\omega_{pitch}[I_y + M_q(\omega_{pitch})] \quad (2.32)$$

$$B_{66v} = \frac{I_z + N_r(0)}{T_{yaw}}, \quad (2.33)$$

where $\Delta\zeta_{heave}$, $\Delta\zeta_{roll}$ and $\Delta\zeta_{pitch}$ represent additional damping in heave, roll and pitch, and ω_{heave} , ω_{roll} and ω_{pitch} are the system's eigenfrequencies in these directions.

The off-diagonal terms cannot be determined analytically with a reasonable degree of accuracy in this case, and are thus omitted.

2.3 Umbilical forces

According to [16], the umbilical cable that connects the ROV to the vessel can be affected by many parameters, including the motions of either the ROV or the vessel, the current along the cable and the total length of the cable itself. The motions of the cable produce forces upon the ROV, which have to be included into the motion equations for it. Thus, the dynamics of the umbilical have to be studied.

The simplest way to model the cable dynamics without losing a large amount of precision is by balancing the forces imposed upon the umbilical upon the currents and motions and the forces the umbilical transfers to the ROV and the operator vessel.

It is assumed that the vertical forces from the current are negligible, which leaves only the horizontal component. Thus, it is possible to use Morison's equation to calculate forces upon the cable [2]:

$$f(u_r) = \frac{1}{2} \rho d C_d |u_r| u_r \quad (2.34)$$

Here, d is the diameter of the cable, C_d is the drag coefficient, ρ is the density of water and u_r is the horizontal current velocity relative to the velocity of the cable. Integrating Equation 2.34 over the length of the cable provides the total force acting upon it. Due to ignoring vertical forces and currents, it is possible to approximate the length of the cable to the height h between the operator vessel and the ROV. Thus:

$$F_d = \int_0^h f(u_r) dz \quad (2.35)$$

Under the influence of the side current, and provided there is slack in the cable, the umbilical will form a curve. Along the curve, there is a point called the vertical tangent point [18]. It denotes the location where no horizontal forces are transferred. This means that above this point, all the horizontal forces must be taken up by the operator ship and below, by the ROV. Thus, the location of the vertical tangent point is decisive in the distribution of the total horizontal forces between the ship and the ROV. See Figure 2.1.

It is assumed that the velocity profile of the current is uniform, which means that the vertical tangent point is located approximately halfway down the cable. Thus, the distribution of horizontal forces between the ROV and the operator vessel is equal. The horizontal force upon the ROV thus becomes $\tau_1 = \tau_2 = -\frac{1}{2} F_d$.

For the vertical component, it is required to consider the total weight of the cable submerged in water ($w_{cable} h$). Using [16], the cable length is assumed to be 20% longer than the height h . Thus, the total heave force is $\tau_3 = 1.2 w_{cable} h$.

Finally, in order to find the pitch and roll moments induced upon the ROV, the arm between the CG and the attachment point for the umbilical has to be found (r_x and r_y). There will be almost no moment in yaw, due to the small arm.

Assembling all the force components into a force vector:

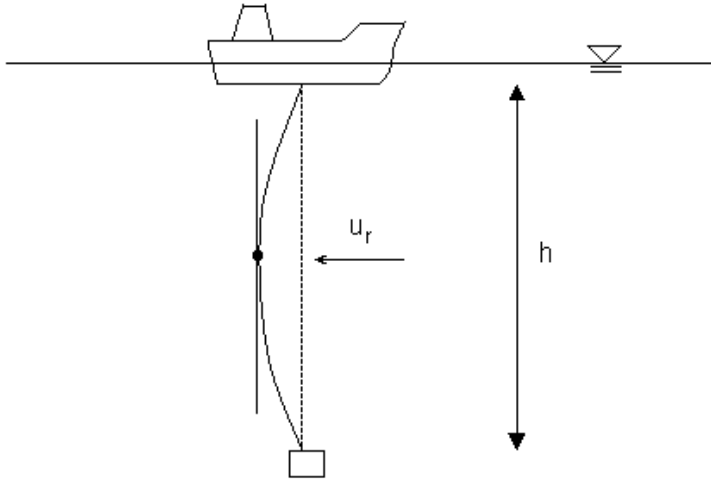


Figure 2.1: The setup of the umbilical cable, with the vertical tangent point shown.

$$\boldsymbol{\tau}_{cable} = \begin{bmatrix} -\frac{1}{4}\rho d C_d \int_0^h |u_r| u_r dz \\ -\frac{1}{4}\rho d C_d \int_0^h |v_r| v_r dz \\ 1.2 w_{cable} h \\ r_z \tau_{cable}(1) \\ r_z \tau_{cable}(2) \\ 0 \end{bmatrix} \quad (2.36)$$

2.4 Control forces

The control forces and moments are the components of the motion equations that execute control over the vessel [2]. In order to find the control force vector, it is necessary to transform the actuator force vector using Equation 2.37.

$$\boldsymbol{\tau} = \mathbf{T}(\boldsymbol{\alpha}) \mathbf{K} \mathbf{u} \quad (2.37)$$

Here, $\mathbf{T}(\boldsymbol{\alpha}) \in \mathbb{R}^{n \times r}$ is the *thrust configuration matrix*, \mathbf{K} is the thrust coefficient matrix, $\boldsymbol{\tau} \in \mathbb{R}^n$ is the control force vector in n DOF, and $\mathbf{u} \in \mathbb{R}^r$ is the actuator input vector consisting of r actuator inputs ([2]). The relation between r and n determines whether the control problem is over-, under- or fully actuated. In the case that $r > n$, the control problem is *overactuated*, in which case an optimization algorithm is needed in the control allocation system, in order to find the optimal control force vector. If $r < n$, the problem is *underactuated*, which leads to the inability to independently control certain DOFs, limiting the control system. Finally, if $r = n$, the control problem is *fully actuated*.

The resulting actuator outputs should be limited by upper and lower bounds depending on the maximum possible performance of the thrusters.

The thrust configuration matrix describes the geometry of the thruster locations on the marine vessel. $\alpha = [\alpha_1, \dots, \alpha_p]^\top \in \mathbb{R}^p$ is a vector of angles for any azimuth thrusters in the system. In the case where no azimuth thrusters are present on the vessel, the thrust configuration matrix becomes static.

Considering that ROV SF 30k has no azimuth thrusters, T for it can be calculated prior to starting the control loop. This requires geometrical data for every thruster, including position and orientation. In this case, spherical coordinates were chosen to describe thruster orientations, where θ is thruster's rotation around the BODY Z-axis, and ϕ is its rotation relative to the BODY XY-plane. With this in mind, it is possible to setup a vector of thruster contribution for every DOF, as shown in Equation 2.38.

$$\mathbf{T}_i = \begin{bmatrix} Surge \\ Sway \\ Heave \\ Roll \\ Pitch \\ Yaw \end{bmatrix} = \begin{bmatrix} \cos \theta \cos \phi \\ \sin \theta \cos \phi \\ \sin \phi \\ -Z \sin \theta + Y \sin \phi \\ -Z \cos \theta + X \sin \phi \\ -Y \cos \theta + X \sin \theta \end{bmatrix} \quad (2.38)$$

These vectors are then assembled into a thrust allocation matrix as shown in Equation 2.39.

$$\mathbf{T} = [T_1, \dots, T_n] \quad (2.39)$$

The thrust coefficient matrix describes the relationship between propeller thrust and shaft speed. Its calculation is shown in Equation 2.40, as given by Carlton [19].

$$\tau = sign(n) K_T \rho D^4 n^2 \quad (2.40)$$

Where K_T is a strictly positive thrust coefficient, ρ is water density, D is propeller diameter and n is shaft speed in rotations per second. Usually, the expression for K_T is found by open water tests. K_T can be expressed by Equation 2.41.

$$K_T = f_1(J_a, \frac{P}{D}, \frac{A_E}{A_O}, Z) \quad (2.41)$$

Where P/D is the propeller pitch ratio, A_E/A_O is the expanded-area ratio, Z is the number of blades and J_a is the advance ratio expressed as such (Equation 2.42).

$$J_a = \frac{V_a}{nD} \quad (2.42)$$

Where V_a is the inflow velocity to the propeller.

In the case that the system has quadratic thrust characteristics, the control vector \mathbf{u} can be defined as shown in Equation 2.43.

$$u_i = |n_i|n_i \quad (2.43)$$

where u_i and n_i are respectively the control component and the shaft speed for thruster i . Conversely, it is easy to find the shaft speed based on known control input:

$$n_i = \text{sign}(u_i)\sqrt{u_i} \quad (2.44)$$

This relation is useful when designing the thrust allocation system, as the ultimate goal of thrust allocation is providing shaft speeds for the actuators based on the force control vector provided by the control algorithm. In this case, Equation 2.37 has to be inverted. The resulting equation is as shown:

$$\mathbf{u} = \mathbf{T}^\dagger \mathbf{K}^{-1} \boldsymbol{\tau} \quad (2.45)$$

Here, $\mathbf{K}^{-1} = 1/\mathbf{K}$ and \mathbf{T}^\dagger is the generalized inverse of the matrix \mathbf{T} . Since the thrust allocation matrix is not necessarily square (in the cases where $n \neq r$), it is not always possible to take a direct inverse of it. The generalized inverse, also called the pseudoinverse [20]. The generalized inverse is calculated as shown in Equation 2.46:

$$\mathbf{T}_w^\dagger = \mathbf{W}^{-1} \mathbf{T}^\top (\mathbf{T} \mathbf{W}^{-1} \mathbf{T}^\top)^{-1} \quad (2.46)$$

where \mathbf{W} is a diagonal weight matrix. In the case where $\mathbf{W} = \mathbf{I}$, the equation is reduced (Equation 2.47):

$$\mathbf{T}_w^\dagger = \mathbf{T}^\top (\mathbf{T} \mathbf{T}^\top)^{-1} \quad (2.47)$$

and is called the *Moore-Penrose pseudoinverse*.

Chapter 3

Modelling of ROV SF 30k

3.1 Vessel model

In this section, the process to evaluate or estimate the parameters of ROV Neptune is shown. Certain parameters can be calculated analytically based on existing documentation, while other parameters cannot be computed directly, and have to be estimated based on either empirical data, or reasonable approximations. A 3-dimensional model of the ROV was provided by Sperre AS. It was designed in AutoCAD. This model was used as a base for calculating several parameters of the model. The programs that were used are SolidWorks, Rhinoceros and WAMIT:

- SolidWorks (version: 2011 x64 bit) - a CAD (computer-aided design) program. In the scope of this thesis, it is used to redesign and simplify the model of ROV SF 30k for use in other programs. It can also be used to set material properties of different elements in the model, which can be used to evaluate weight, mass center, or moment inertia of the model.
- Rhinoceros 3D (version: 4.0) - a NURBS (Non-uniform rational basis spline) based 3D modelling program. In the context of this thesis, it is used as a tool to transform the NURBS-based 3D model of the ROV into a polygon mesh that can be analyzed in programs based on numeric algorithms, like WAMIT.
- WAMIT (version: v6) - a program for calculating motions and loads upon offshore structures in waves. Despite it being primarily used for surface structures in the wave zone, it can still be used to calculate certain parameters of underwater vessels that operate outside of the wave zone. These parameters include, amongst others, added mass coefficients, buoyancy and center of buoyancy.
- MATLAB (version: R2011b) - this program is mainly used as an assistance for calculations. Several helping routines have been written in MATLAB script, particularly for dealing with the added mass coefficient matrix.

3.1.1 Mass and added mass calculations

All of the parameters in this section were evaluated using the aforementioned programs. A detailed description of the usage of each program is outlined below.

SolidWorks

The program SolidWorks was used for several purposes, mainly for finding the rigid body matrix and center of gravity, as well as for simplifying the model to a degree that could be analyzed by WAMIT. The version of the program that was used was SolidWorks 2011 x64 edition.

The first step was importing the AutoCAD drawing into the program. It had to be converted to a SolidWorks compatible format. This generated an assembly with several parts, where every thruster is considered a separate part. In addition, the two electrical cylinders in the middle of the ROV are separate parts as well. The last part is the remaining structure of the ROV, including the floating element, the frame and the small components attached to it.

The unedited model was then used to calculate the rigid body matrix of the ROV. An assumption was made that most of the features in the 3D model consist of steel. The amount of rubber or plastic components is insignificant in this case, and the assumption is then considered sufficiently accurate. Thus, every single component was converted to the material “Plain Carbon Steel”. After that, the mass properties of the ROV were evaluated. This provided several key parameters, namely the mass, volume, center of gravity and moments of inertia at the origin and at the center of gravity. Finally, the ROV was moved such that its center of gravity coincided with the origin of the coordinate system. This significantly simplified several future calculations, as well as the WAMIT simulations. The unedited but converted model can be found in Appendix B.A.

The next step was simplifying the model in order to make it feasible for hydrodynamic calculations in WAMIT. SolidWorks has a feature recognition system called FeatureWorks. Its purpose is analysis of an imported structure, and its breakdown into elementary components that can be modified within the program (features, sketches, reference geometry). However, due to the complexity of the ROV, as well as overlapping of components in several places, FeatureWorks was not able to analyze the structure properly. Thus, most of the editing had to be done manually. This was performed in several steps:

1. Removal of unnecessary components - features such as small flat beams, or structures embedded into the floating element from below. Such components have no significant effect on the hydrodynamic properties, and can thus be removed without severely altering the results of the WAMIT simulations.
2. Breakdown and simplification of all the thrusters and electrical cylinders. Unlike the main ROV frame, the parts featuring the thrusters of the ROV were simple enough to be analyzed using FeatureWorks. The thrusters were stripped of most of their elements, including the entirety of the electrical engines (since those are embedded into the floating element, and can be

assumed to have little influence on hydrodynamic properties of the ROV). Furthermore, at a later stage, it was found out that the fine cylindrical shapes of the thrusters did not mesh very well, and created various problems in WAMIT analysis (more on that later), which is why they were reduced to hollow octagonal cylinders.

3. Simplification of the floating element - due to the way it was designed, the floating element was imported as a single continuous surface into SolidWorks. Thus, it had to be rebuilt from ground up. In the process, any irregularities on its bottom (where it connects to the rest of the ROV structure) had been smoothed out, as a compensation for the removal of embedded components, and to further reduce the polygon count of the model. The thruster housing tunnels were remodeled to be octagonal as well.
4. Simplification of the ROV frame - most of the beams used in the construction of the ROV had the U-profile. These were replaced with solid beams with the same outward dimensions. The small cylinder in the front of the ROV was also reduced to an octagonal profile.

Figures 3.1 and 3.2 show the result of the simplification process performed on the model:

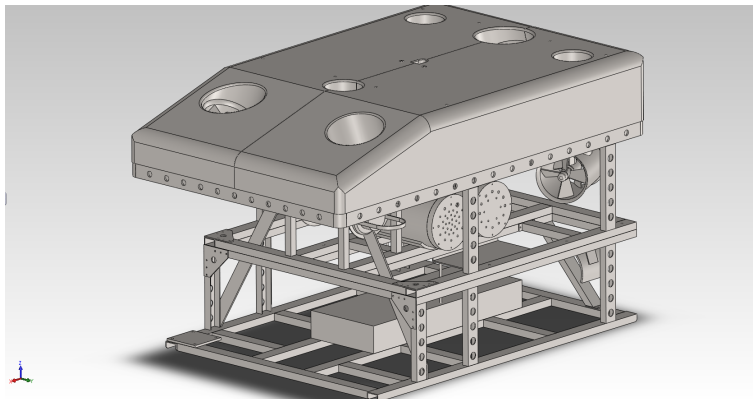


Figure 3.1: Original AutoCAD model with added weight emulating sensory systems.

It should be noted that the boxes on the bottom of the model are not the same size. This is due to the fact that the models are used for different purpose. The small box in the original model (top) serves as a way to estimate the approximate weight and moments of inertia of installed sensory equipment on SF 30k, without regards to its volume. The large box on the simplified model represents an approximate volumetric equivalent of the equipment, and is used for volume (and thus buoyancy) and added mass calculations in WAMIT. The simplified model is located in Appendix B.B.

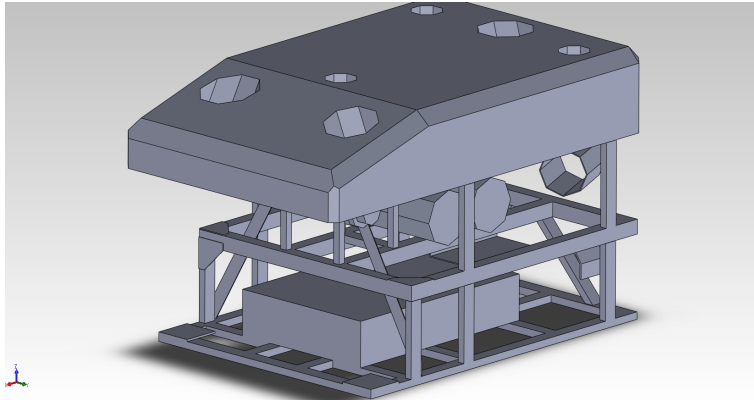


Figure 3.2: Simplified model intended for WAMIT analysis.

Conversion to WAMIT through Rhinoceros

Analyzing a model in WAMIT requires the input model to be converted to a mesh and saved in a compatible file format. SolidWorks can perform neither of those actions, which is why a secondary program is used. In this case, Rhinoceros 4.0 (henceforth named Rhino) was used. First, the simplified model was saved in SolidWorks as a .STEP file. This file was then opened in Rhino, and the model was then meshed using the meshing tool. The .STEP file (along with the Rhinoceros .3DM file as a backup) is located in Appendix B.C.

SolidWorks does not operate with polygon meshes, but rather with NURBS objects (Non-uniform rational basis spline), which use curves and continuous curved surfaces to generate objects in 3D. When meshing curved objects, a very high resolution of a mesh is required to avoid geometrical artifacts. This leads to unnecessary amounts of polygons, increasing WAMIT simulation times dramatically. This is the primary reason for reducing all cylinders in the ROV model to octagons. Doing that made it possible to mesh the ROV with the lowest possible resolution without sacrificing geometry detail, but reducing simulation time to just a few minutes.

The resulting polygon mesh was saved as a .GDF file, compatible with WAMIT. The heading of the file indicates that the mesh consists of 1484 polygons. It is also worth noting that during the conversion of the model in Rhino, the unit system was changed from millimeters to meters. The converted .GDF file can be found alongside other WAMIT files in Appendix B.D

WAMIT simulation

WAMIT is a specialized program designed for calculating hydrodynamic wave loads and motions on offshore structures. Despite being primarily used for wave calculations, it can also be used to find added mass coefficients for underwater vessels outside of the wave zone provided a proper set of rules to use. The program must

be run through either a command prompt, or through a BATCH file, and the settings and parameters of the simulation are stored in several files. Below is a list of those files, as well as the settings used for calculation of added mass and buoyancy of ROV SF 30k. The documentation on setting up those files was found in [21]

- *SF 30k.GDF* - the Geometric Data File. This file describes the polygon mesh that the simulated object is described by. For SF 30k, the file was generated by Rhino using the roughest polygon mesh settings possible.
- *SF 30k.FRC* - the Force Control File. This file stores the parameters for the FORCE subprogram of WAMIT. This file has 2 different forms (alternative 1 and alternative 2). This is determined in the configuration file (.CFG), and the form decides which parameters the file includes. In this case, alternative form 2 was used.

The first 9 integers indicate the hydrodynamic parameters that can be calculated using this subprogram. For SF 30k, only the parameter 1 was chosen to be calculated. The rest of the parameters are irrelevant outside of the wave zone. The first parameter describes added mass and damping coefficients. It should be noted that the damping coefficient only describes potential damping resulting from wave forces, and is not calculated if the wave period is 0 or infinite.

Aside from the hydrodynamic parameters, the file stores information on the physical parameters of the simulated body. The 3 numbers below the water density (RHO) denote the center of gravity of the object relative to the center of origin for the simulation (to be determined in the potential control file, .POT). Due to the fact that the ROV is centered at its geometric center of mass in the 3D modelling programs, the CG vector is [0 0 0] in this case.

The next block of data stores the 6x6 rigid body mass matrix of the body. In this case, the results of Mass Property evaluation of the original, unedited model in SolidWorks were used. It is remarkable that the resulting rigid body mass matrix is very similar to the one calculated on the rough model in the Fall 2011 project. The last four numbers determine, respectively:

- *IDAMP* - the inclusion of the internal damping matrix, in this case 0.
- *ISTIFF* - the inclusion of the internal stiffness matrix, also 0.
- item *NBETAH* - the amount of Haskind wave headings to be simulated. Since wave forces are not relevant for this simulation, the number is set to 0 as well.
- *NFIELD* - the amount of points at the surface of the fluid domain to be evaluated. Also 0 due to irrelevance.
- *SF 30k.POT* - the Potential Control File. This file determines the parameters input into the POTEN subprogram of WAMIT. Just like the Force Control File, it has 2 alternative forms. Alternative form 2 was used for this file.

The parameters input into this file control the potential flow in the simulation, including wave behavior, body positions, water depth as well as specification on whether the radiation and diffraction problems are to be solved.

The first number (*HBOT*) specifies dimensional water depth. This parameter is relevant when waves are included into calculations. In the case of SF 30k, since at this stage it operates outside of the wave zone, this parameter can be chosen arbitrarily, in this case it's 50m.

The second line with two numbers (*IRAD*, *IDIFF*) controls whether radiation and diffraction problems are going to be solved during simulation. Both options have 3 settings: -1 (do not solve the problem), 0 (solve the problem only for specified degrees of freedom) and 1 (solve the problem for all degrees of freedom). At least one of the problems must be solved for the simulation to give any results. In this case, both options have been set to 1.

The next four numbers determine the wave periods and headings in the simulation:

- *NPER* - the amount of different wave periods, in this case 1.
- *PER* - array of wave periods. Setting it to 0 will assume a wave period of 0, and -1 assumes a wave period of infinity.
- *NBETA* - the amount of incident wave headings, again, 1.
- *BETA* - array of wave headings. The only heading specified is 0 degrees.

The last part of the .POT file determines the properties of the simulated body or bodies. *NBODY* specifies how many separate bodies are involved in the simulation, each requiring its own .GDF file. The name of the .GDF file is on the next line, in this case it's SF 30k.gdf.

The line of four numbers below the .GDF name (*XBODY 1*) specifies the X, Y, Z coordinates of the first body, as well as its heading relative to the coordinate system used in WAMIT. It should be noted that WAMIT uses the right-hand rule, but unlike most hydrodynamic calculations involving the earth-reference frame, Z is positive upwards and not downwards. Thus, the Z coordinate of -5 used for the SF 30k denotes that it is located 5m below surface of the water. The depth of the ROV is not relevant in this case, so long as it is completely submerged, since there are no wave forces acting upon it.

MODES BODY 1 determines which degrees of freedom the diffraction and/or radiation problems should be calculated for. In this case, all the DOFs are chosen to be evaluated.

Finally, the *NEWMDS* line is defined as “the number of generalized modes for Kth body” (reference: WAMITv6.4 manual). In most cases, this option is set to 0, but must be included in the .POT file regardless of the setting, just like *NBODY*.

- *SF 30k.CFG* - the Configuration File. This is the master configuration file, which controls most of the top-level parameters of the simulation, as well as determines which forms of .POT and .FRC are to be used in the simulation. Below is the list of options in the file:
 - *IPLTDAT* determines whether a file containing panel and patch data is generated. Due to its irrelevance to this simulation, it is set to 0.
 - *MAXSCR* specifies the allotted RAM for scratch storage for POTEN.
 - *IFORCE* and *IPOTEN* determine whether the FORCE and POTEN subprograms should run. Both are set to 1.
 - *IALTFRC* and *IALTPOT* determine which forms of .FRC and .POT files are used. Both are 2 in this case, as specified in the individual file analyses earlier.
 - *MAXITT* determines the maximum amount of iterations POTEN should run. This is generally determined by the complexity of the model. The number 100 is probably unnecessary large for the relative simplicity of the ROV calculations, but it's preferable to have a number too large, rather than too small.
 - *ISOLVE* determines which solver should be used. *ISOLVE=0* uses the iterative solver. The next several parameters (*ISCATT*, *IQUAD*, *ILOG*, *IDIAG*, *IRR*) calibrate the operation of the solver in POTEN. The values chosen in the case of SF 30k are determined not to affect the results of the simulation with any significance.
 - *MONITR* and *NUMHDR* operate with data output, and are not necessary to be changed, due to all the required data being output to separate files.
 - *USERIDPATH* is standard installation procedure, and should be modified according to the installation path for WAMITv6.
- *fnames.WAM* - File Name Manager File. This file determines which files are involved in the simulation. All of the above files are included in it.
- Simulation output - WAMIT outputs its data into several files, including an .OUT file, a .HST file, a .PNL file (determined by *IPLTDAT*) and .* files, where * corresponds to the number of the option chosen in the .FRC file. In the case of the simulation of SF 30k, the following files were output:
 - *SF 30k.out*
 - *SF 30k.hst*
 - *SF 30k.1*

All the required parameters can be extracted from the .OUT file, namely the center of buoyancy (Xb, Yb, Zb), which is determined to be:

$$\mathbf{r}_b = [0.0822 \quad -0.00773 \quad 0.3872] \quad (3.1)$$

However, the main purpose of the simulation is the added mass coefficient matrix. WAMIT outputs the matrix on a per-element basis, which must further be edited into a single matrix. Using a simple MATLAB script (also included in Appendix B.D), the added mass matrix is properly formatted.

It is worth noting a peculiar tendency of WAMIT to output an asymmetrical added mass matrix. The values on the opposite sides of the main diagonal are not equal, even though they should be. This problem persisted with every single simulation performed in WAMIT, even ones performed on a simple cube. Thus, the MATLAB script performs an additional function of averaging out the off-diagonal values. The resulting added mass matrix is symmetric, but must be multiplied by water density before being able to be used in simulators or observers.

The results of the simulations led to the following rigid body and added mass matrices:

$$\mathbf{M}_{RB} = \begin{bmatrix} 1862.87 & 0 & 0 & 0 & 0 & 0 \\ 0 & 1862.87 & 0 & 0 & 0 & 0 \\ 0 & 0 & 1862.87 & 0 & 0 & 0 \\ 0 & 0 & 0 & 525.39 & 1.44 & 33.41 \\ 0 & 0 & 0 & 1.44 & 794.20 & 2.60 \\ 0 & 0 & 0 & 33.41 & 2.60 & 691.23 \end{bmatrix} \quad (3.2)$$

$$\mathbf{M}_A = \begin{bmatrix} 779.79 & -1.3053 & -94.244 & 14.652 & -165.06 & -6.7288 \\ -12.449 & 1222 & 124.5 & 436.34 & -20.566 & 59.971 \\ -112.4 & -21.919 & 3659.9 & -33.129 & -382.17 & -12.571 \\ 2.433 & 382.55 & 45.351 & 534.9 & -13.53 & 7.9038 \\ -166.02 & 8.868 & -390.67 & -6.5248 & 842.69 & 0.16383 \\ -8.8778 & 65.481 & 34.121 & 34.133 & -2.4007 & 224.32 \end{bmatrix} \quad (3.3)$$

Using the MATLAB script, the matrix was symmetrized to the following:

$$\mathbf{M}_A = \begin{bmatrix} 779.79 & -6.8773 & -103.32 & 8.5426 & -165.54 & -7.8033 \\ -68.773 & 1222 & 51.29 & 409.44 & -5.8488 & 62.726 \\ -103.32 & 51.29 & 3659.9 & 6.1112 & -386.42 & 10.774 \\ 8.5426 & 409.44 & 6.1112 & 534.9 & -10.027 & 21.019 \\ -165.54 & -5.8488 & -386.42 & -10.027 & 842.69 & -1.1162 \\ -7.8033 & 62.726 & 10.775 & 21.019 & -1.1162 & 224.32 \end{bmatrix} \quad (3.4)$$

3.1.2 Damping

Nonlinear damping

Unlike added mass, it is much harder to determine the damping coefficients for a vessel without performing towing tests and determining the damping experimen-

tally. However, model-scale tests were performed on ROV Minerva. Minerva and SF 30k share many similarities, including the relative dimensions and approximate shape. Thus, it is possible to estimate the nonlinear damping coefficients for SF 30k based on those of Minerva with a decent degree of accuracy. According to [16], the nonlinear damping coefficients for Minerva are as follows:

$$\mathbf{C}_{d,NL}(Minerva) = \begin{bmatrix} 0.87 \\ 0.99 \\ 1.05 \\ 1.00 \\ 1.00 \\ 1.00 \end{bmatrix} \quad (3.5)$$

In order to convert them into a nonlinear damping matrix, these coefficients have to be multiplied by projected area of the ROV in surge, sway, heave and along the axes of rotation of the ROV. The projected area was calculated in SolidWorks (The relevant files are located in Appendix B.E). A rough sketch of an area was drawn in every DOF. The sketch was then converted into a feature (extruded boss in this case), and its projected area was measured using the “Measure” tool. The resulting projected areas are as follows:

$$\mathbf{A}_{proj} = \begin{bmatrix} 1.6781 \\ 1.9562 \\ 3.3840 \\ 4.3107 \\ 3.8449 \\ 2.6410 \end{bmatrix} [m^2] \quad (3.6)$$

These values make it possible to calculate nonlinear damping in translational DOFs using Morrison’s equation:

$$D_{NL} = \frac{1}{2} \rho C_d A_{proj} |v_r| \quad (3.7)$$

Thus, the nonlinear translational damping coefficients were found to be:

$$\mathbf{D}_{NL,trans} = diag\{748.22|u_r|, 992.53|v_r|, 1821.01|w_r|\} \quad (3.8)$$

However, this method is not applicable to rotational DOFs. It was thus decided to scale up the nonlinear damping values from ROV Minerva. According to [16], the nonlinear damping values for ROV Minerva are:

$$\mathbf{D}_{NL} = diag\{292|u_r|, 584|v_r|, 635|w_r|, 84|p|, 148|q|, 100|r|\} \quad (3.9)$$

The last three values are scaled up using the scaling factors found by comparing the dimensions of the two ROVs. According to [22] and Appendix A, the two ROVs have the dimensions outlined in Table 3.1.

Scaling was performed based on geometric similarity [23], using the largest applicable scale factor. The formula used is as follows:

$$F_s = \frac{\rho_s}{\rho_m} \lambda^3 F_m \quad (3.10)$$

where ρ_s and ρ_m are water density for full-scale ship and the model respectively, and λ is the scaling factor. This equation is used to scale up forces from model tests to ship dimensions, but here, it can be used to scale dimensions from Minerva up to SF 30k. In this case, F_s denotes the nonlinear damping forces for SF 30k, while F_m denotes the same forces for Minerva.

Using 3.1.2, 3.9 and 3.10, the following rotational nonlinear damping coefficients were found:

$$\mathbf{D}_{NL,rot} = diag\{672|p|, 774.44|q|, 523.27|r|\} \quad (3.11)$$

Combining 3.8 and 3.11, the following nonlinear damping matrix is achieved:

$$\mathbf{D}_{NL} = \begin{bmatrix} 748.22|u_r| & 0 & 0 & 0 & 0 & 0 \\ 0 & 992.53|v_r| & 0 & 0 & 0 & 0 \\ 0 & 0 & 1821.01|w_r| & 0 & 0 & 0 \\ 0 & 0 & 0 & 672|p| & 0 & 0 \\ 0 & 0 & 0 & 0 & 774.44|q| & 0 \\ 0 & 0 & 0 & 0 & 0 & 523.27|r| \end{bmatrix} \quad (3.12)$$

Linear damping

Linear viscous damping is harder to estimate than its nonlinear counterpart, and often requires model scale or full scale tests. For Minerva, the damping forces were found by bollard pull tests of the ROV, where the pulling force loss is compared to quadratic damping calculated previously. The force loss was larger than estimated by the nonlinear damping equations, and the remainder was thus attributed to linear damping forces. The linear damping matrix was then estimated based on this. The linear damping coefficients were estimated as a percentage of the nonlinear ones, as follows [16]:

Table 3.1: Dimension and scale comparison of ROV Minerva and ROV SF 30k.

Dimensions[m]		Scale
Minerva	SF 30k	λ
1.44	2.50	1.7361
0.82	1.50	1.8293
0.80	1.60	2.0000

$$\mathbf{D}_L = \text{diag}\left\{\begin{bmatrix} 10\% \\ 7\% \\ 40\% \\ 40\% \\ 40\% \\ 20\% \end{bmatrix}\right\} \mathbf{D}_{NL} \quad (3.13)$$

Due to the lack of test data for ROV SF 30k, the most accurate method of calculating linear viscous damping would be to use the linear damping correlations from ROV Minerva. These values can be calibrated once sea trials begin. Thus, the linear damping coefficient matrix for SF 30k is calculated to be:

$$\mathbf{D}_L = \begin{bmatrix} 74.82 & 0 & 0 & 0 & 0 & 0 \\ 0 & 69.48 & 0 & 0 & 0 & 0 \\ 0 & 0 & 728.40 & 0 & 0 & 0 \\ 0 & 0 & 0 & 268.80 & 0 & 0 \\ 0 & 0 & 0 & 0 & 309.77 & 0 \\ 0 & 0 & 0 & 0 & 0 & 105.00 \end{bmatrix} \quad (3.14)$$

3.1.3 Restoring forces and moments

One of the parameters output in the WAMIT .OUT file is the volume of the vessel. The data, just like buoyancy data, can be found in the header of the file. Any of the three calculated volumes can be used. Thus, the volume displacement of the ROV is found to be $VOLX = \nabla = 1.83826m^3$. Multiplying it by the density of sea water and then by the gravitational constant, it is possible to obtain the buoyancy force upon the ROV when fully submerged: $B = \rho\nabla g = 1025 \cdot 1.83826 \cdot 9.81 = 18484.168N$. The weight of the ROV is $W = mg = 1862.87 \cdot 9.81 = 18274.75N$. Thus, the net difference is $B - W = 18484.16 - 18274.75 = 209.4N$. This difference is a bit too large, and is most likely caused by rounding errors due to the fact that the volume of the ROV was calculated using a simplified model.

The restoring forces are calculated based on the relative positions of the center of gravity and the center of buoyancy. Since the ROV is positioned such that its center of gravity is at the center of origin, the following applies:

$$\mathbf{r}_{CG} = \begin{bmatrix} 0 \\ 0 \\ 0 \end{bmatrix} [m], \mathbf{r}_{CB} = \begin{bmatrix} 0.0822 \\ -0.0077 \\ 0.3872 \end{bmatrix} [m] \quad (3.15)$$

3.1.4 Umbilical forces

According to Appendix A, the diameter of the umbilical is 27mm, that is, $d = 0.027m$. The drag coefficient is assumed to be $C_d = 1.2$. The cable weight is not given, however, the cable can be assumed to be approximately neutrally buoyant, due to being designed for use underwater.

The attachment point of the cable is assumed to be at the top of the ROV, approximately directly above the CG. Thus, $r_x = r_y \simeq 0$. Using the 3D model of the ROV, the vertical arm was found to be $r_z = 0.9317m$.

Assuming uniform current speed u_r , it is possible to set up the following umbilical force vector:

$$\boldsymbol{\tau}_{cable} = \begin{bmatrix} -8.3025h|u_r|u_r \\ -8.3025h|v_r|v_r \\ 0 \\ 7.7354h|u_r|u_r \\ 7.7354h|v_r|v_r \\ 0 \end{bmatrix} \quad (3.16)$$

3.2 Thrust allocation

Modelling thrust allocation for an ROV involves calculating three main parameters: the thrust allocation matrix T , which specifies the configuration of the thrusters on the vessel; the thrust coefficient matrix, which establishes dependencies between applied thruster RPM and the resulting thrust; and finally, the thrust loss coefficients, which compensate for any thrust losses affecting the propulsion system of the vessel. Unfortunately, it is impossible to find thrust losses without any kind of empirical data, and thus they will have to be estimated.

3.2.1 Thrust configuration matrix

For ROV SF 30k, it is possible to calculate the thrust configuration matrix based on the model provided by Sperre, since this matrix is based purely on geometric data. Unfortunately, the thrust allocation subroutine in the control system requires the thruster data to be input in a specific order, which is impossible without actual trial and error. Thus, for the purposes of this document, the thrusters were given their IDs arbitrarily, with the possibility of switching out their IDs later.

SF 30k has 6 thrusters, which means that it is fully actuated. Figures 3.3, 3.4 and 3.5 show the positions and orientations for all the thrusters.

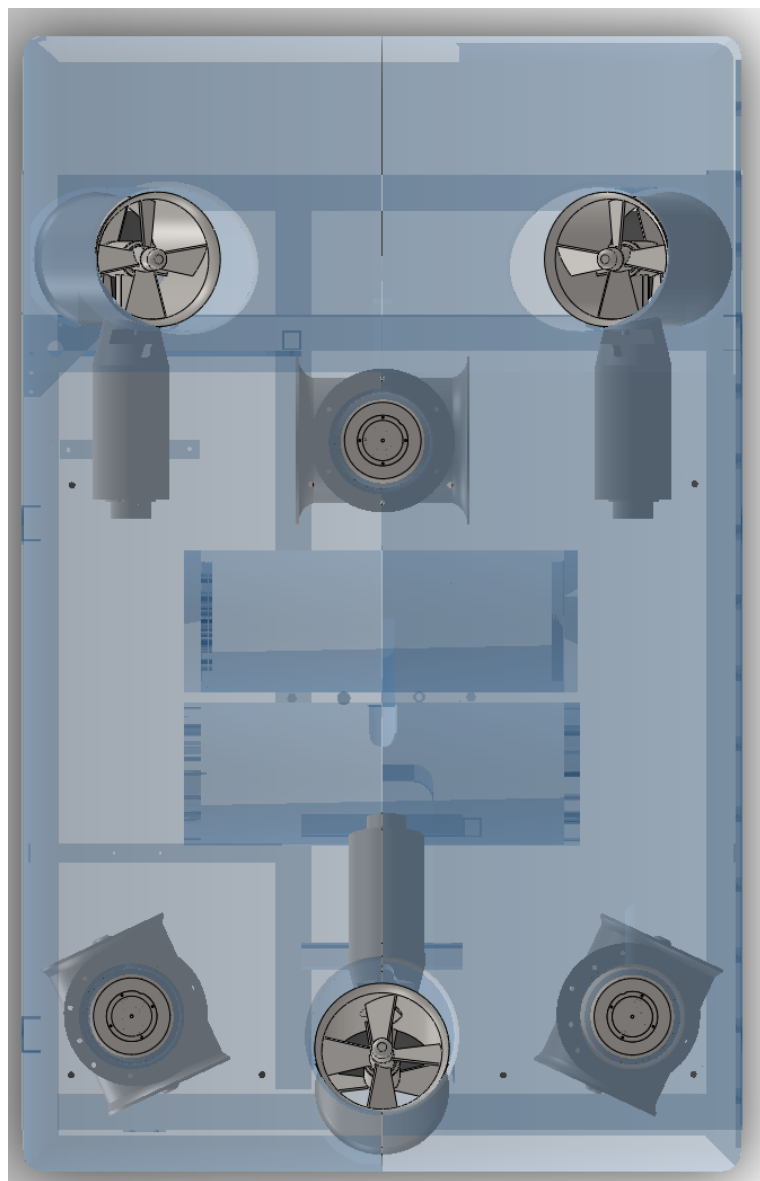


Figure 3.3: ROV thruster positions, top view.

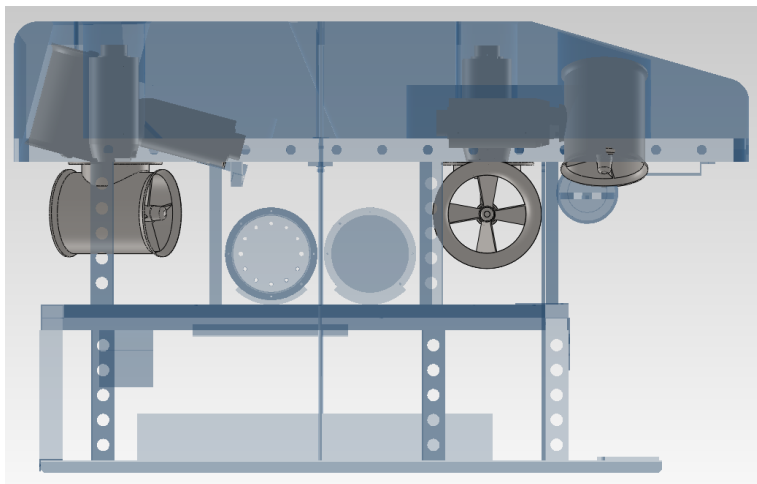


Figure 3.4: ROV thruster positions, side view.

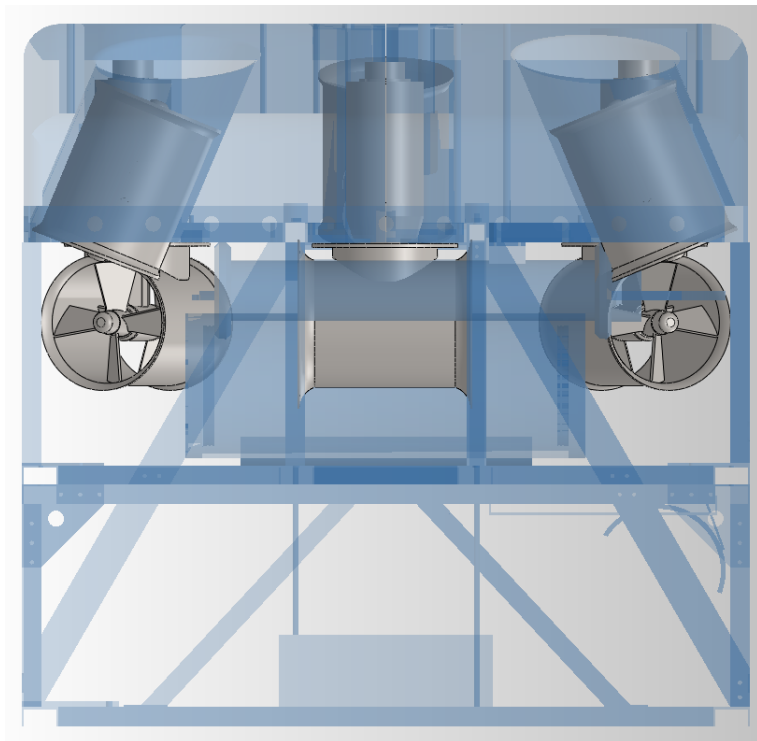


Figure 3.5: ROV thruster positions, front view.

The preliminary IDs have been given to the thrusters based on the top view, shown in figure 3.6.

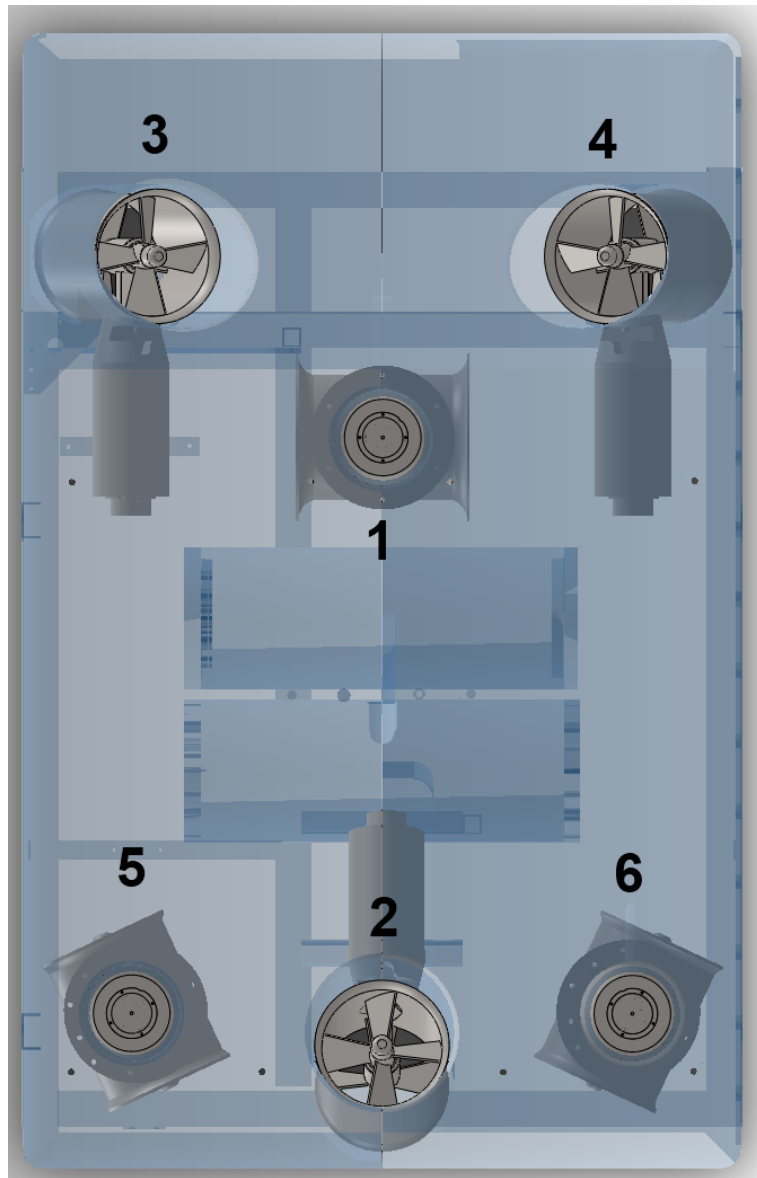


Figure 3.6: ROV thruster IDs.

The positions and orientations of all the thrusters were found by measuring them in SolidWorks using the “Measure” tool, relative to the center of gravity (which coincides with the center of origin of the model). Thruster orientation data was output in spherical coordinates relative to body center of origin, as this significantly simplified the setup of thrust allocation. A table reflecting the measurements is shown in Table 3.2.

Table 3.2: Thruster positions and orientations for ROV SF 30k.

Thruster ID	Thruster position			Thruster orientation	
	X[m]	Y[m]	Z[m]	θ [deg]	ϕ [deg]
1	0.4878	0	-0.2373	-90	90
2	-0.8217	0	-0.5890	0	15
3	0.8654	-0.5322	-0.5332	90	22.5
4	0.8654	0.5322	-0.5332	-90	22.5
5	-0.7076	-0.5129	-0.2404	-25	90
6	-0.7076	0.5129	-0.2404	25	90

The coordinates are given in the BODY coordinate system, with the X axis pointing forward, the Y axis pointing to the starboard (right) side and the Z axis pointing downward. The angle θ is measured as a rotation about the Z axis, positive when clockwise if looking from above. The angle ϕ is measured as a rotation away from the Z axis, with 0° being pointing straight down, 90° being horizontal and 180° straight up.

It is worth noting that all the thrusters have a negative Z coordinate, that is, they are located above the center of gravity of the ROV. This will create a net pitch or roll moment when moving in horizontal degrees of freedom. However, the ROV’s high restoring moment will prevent it from pitching or rolling to a significant degree.

Another noteworthy mention is that the control box installed on SF 30k does not allow control of individual vertical thrusters. Instead, they are combined into a single “vertical thruster”. Thus, the thrust allocation system must reflect this limitation. Thrusters 2, 3 and 4 are combined into a single thruster. The position of their combined thrust force vectors is calculated as an average of thrust contributions of every thruster. Since thrusters 3 and 4 face in opposite horizontal directions (positive and negative in sway), they offset each other’s contribution in sway, and their orientations θ and ϕ can be assumed to be 0° and 90° respectively. The average of the positions and orientations for the combined thruster can now be calculated using equations outlined in 3.17.

Table 3.3: Thruster positions and orientations with combined vertical thrusters.

Thruster ID	Thruster position			Thruster orientation	
	X[m]	Y[m]	Z[m]	θ [deg]	ϕ [deg]
1	0.4878	0	0.2373	90	90
2	0.2862	0	0.5518	0	5
3	-0.7076	-0.5129	0.2404	-25	90
4	-0.7076	0.5129	0.2404	25	90

$$\begin{aligned}
 X_{vert} &= \frac{\sum_{i=2}^4 X_i}{i} \\
 Y_{vert} &= \frac{\sum_{i=2}^4 Y_i}{i} \\
 Z_{vert} &= \frac{\sum_{i=2}^4 Z_i}{i} \\
 \theta_{vert} &= \frac{\sum_{i=2}^4 \theta_i}{i} \\
 \phi_{vert} &= \frac{\sum_{i=2}^4 \phi_i}{i}
 \end{aligned} \tag{3.17}$$

Here, X_i , Y_i , Z_i , θ_i and ϕ_i are the position and orientation data for thruster ID i .

The rest of the thrusters that come after the combined vertical thruster have had their thruster IDs shifted so as to match the reduced thruster count. Thus, the modified thrust ID Table 3.3 is set up.

The geometrical data is input into the control system, which calculates the thrust allocation matrix according to Equation 2.38. This is repeated for every thruster in sequence. The vectors are then inserted into the matrix. The result is as shown in Equation 3.18.

$$\mathbf{T} = \begin{bmatrix} 0 & 0.0872 & 0.9063 & 0.9063 \\ 1 & 0 & -0.4226 & 0.4226 \\ 0 & 0.9962 & 0 & 0 \\ -0.2373 & 0 & -0.4113 & 0.4113 \\ 0 & -0.2815 & 0.2179 & 0.2179 \\ 0.4878 & 0 & 0.7639 & -0.7639 \end{bmatrix} \tag{3.18}$$

3.2.2 Thrust coefficient matrix

The thrust coefficient matrix for SF 30k is derived from the thrust-RPM curves provided by Sperre AS (Appendix C). According to Sperre AS, the thruster model used in SF 30k is Sleipner SP 125 T. The thrust-RPM curve in Appendix C is labeled as SE 120, which is what is going to be used in the calculation of thrust coefficient data. No data for maximum RPM was given for the thrusters, and it is

thus assumed that it is similar to the RPM boundaries for ROV Minerva [24], and is set to be 1500.

The curve is quadratic, and thus the coefficient matrix is not constant. However, it is possible to derive a simple equation for the curve based on the provided data. This is performed by regressing the graph in MATLAB, and then using the found coefficients in a second-degree equation shown in 3.19.

$$\tau = A \cdot RPM^2 \quad (3.19)$$

where A is the quadratic coefficient to be found through regression.

Quadratic regression requires at least 3 uniquely defined entries in the data set that is to be regressed. For the sake of simplicity, the graph endpoint (2300, 1540) was used as one of the entries. This point was then mirrored across the Y-axis, to get the point (-2300, 1540). Including the point of origin (0, 0) and regressing the resulting data set will result in a parabolic curve, where the section of it to the right of the Y-axis (positive X-values) is the regressed thrust-RPM curve. It should be noted that the section of the curve to the left of the X-axis does not reflect the physical behavior of the thruster, but is merely included to provide a 3rd unique point for curve regression.

The data set was defined as two vectors in MATLAB, and can be seen in Equation 3.20.

$$RPM = \begin{bmatrix} -2300 \\ 0 \\ 2300 \end{bmatrix}, \tau = \begin{bmatrix} 1540 \\ 0 \\ 1540 \end{bmatrix} \quad (3.20)$$

These vectors were plotted using the “plot” command and then fitted with a quadratic function to find the coefficients. Figure 3.7 shows the regression process of the thrust-RPM curve.

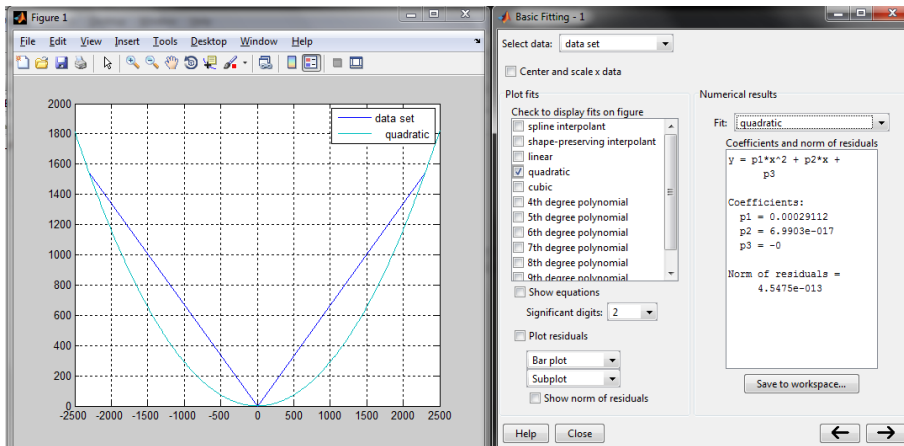


Figure 3.7: The regressed thrust-RPM curve and the fitted coefficient.

As can be seen from the figure, the coefficient was found to be $A = 0.00029112$. Thus, the final RPM-to-thrust equation is shown in Equation 3.21.

$$\tau = 0.00029112 \cdot RPM^2 \quad (3.21)$$

3.2.3 Thrust loss

Unfortunately, no towing tests were performed on ROV SF 30k, and as such, there is no thrust loss data accumulated for this ROV. Therefore, a preliminary set of conservative thrust loss coefficients was used in the scope of the project. Every thrust loss factor was set to 40%, as shown in Equation 3.22.

$$C_l = \begin{bmatrix} 0.4 \\ 0.4 \\ 0.4 \\ 0.4 \\ 0.4 \\ 0.4 \\ 0.4 \end{bmatrix} \quad (3.22)$$

Chapter 4

Control system

The control system for ROV Neptune was developed in LabVIEW, which is a graphical programming language not too dissimilar to MATLAB Simulink. The development of the program is outlined in Master's Thesis by Espen Tolpinrud [1]. This chapter outlines the development and modification of individual sections of the control system on the plant control layer (see Figure 1.3).

4.1 6DOF adaptation

The original system, which was tailor-made for ROV Minerva, was limited by the fact that it operated in 4 DOFs. One of the goals of this thesis was to deliver a more generalized system, one which is able to provide fully actuated control in all 6 DOFs. Most of the main elements of the system had to be modified to be able to provide additional control in pitch and yaw, including the observer, the controller(s), the tracking/guidance subsystems and the thrust allocation system.

4.1.1 Observers

Sector Kalman Filter

The Kalman Filter observer from the old system has been translated to the new structure. The output is transformed to work with a 6DOF system. However, the observer is not actually 6DOF.

The linearization has only been done with respect to 36 different yaw angles. If this were to be done for both roll and pitch as well, the initialization would need to iterate and store values from 36^3 iterations for a sampling interval of 10 degrees in each rotation direction. The performance requirement needed can be calculated by the following formulas:

$$N \times \varpi = \text{Memory requirement} \quad (4.1)$$

N is the number of elements to be stored and ϖ is the data size. The processor usage can be found by identifying FLoating-point OPerations (flop) in the routine and how many FLoating-point Operations Per Second (flops) the processor is capable to perform.

$$\sigma_{flop} \times n_{iter} = flop \quad (4.2)$$

$$\chi \times_{core} \times n_{core} = flops \quad (4.3)$$

$$\frac{flop}{flops} = t \quad (4.4)$$

σ is the number of flop per iteration, n is the number of iterations. In Equation 4.3 χ is number of flop the processor is able to perform on each cycle. On modern processors this is usually 4. f is the clock frequency or cycle frequency of the processor, and m is the number of cores available on the processor.

$$(2 \times (18 \times 36^3 \times 18) + 18 \times 36^3 \times 6) \times 8 B = 282175488 B \cong 282 MB \quad (4.5)$$

The expression in Equation 4.5 applies for the linearization matrices Φ , Γ and Δ in the Kalman Filter. 282 MB free memory is needed for each Kalman Filter object initialized in the system in order to store these matrices.

$$6943 \frac{flop}{iteration} \times 36^3 iterations = 323932608 flop \quad (4.6)$$

$$4 \frac{flop}{cycle} \times 1.6e9 \frac{cycles}{second} \times 4 cores = 25.6e10 flops \quad (4.7)$$

$$\frac{323932608 flop}{25.6e9 flops} \cong 0.01 seconds \quad (4.8)$$

The values in Equation 4.3 is based on the authors PC which has a Intel i7-720QM [25], hence the numeric result in Equation 4.4 is only valid for this processor. It should however be noted that the difference in run-time performance for the different processors is of $O(10^{-2})$, hence the calculation time for the matrices can be neglected.

With the results given in Equations 4.5 and 4.8 there should in theory be no problem running a 6DOF linearized Kalman Filter on a modern PC. However, the system performance may be reduced due to large memory operations, especially if global variables are used [26], [27].

Passive non-linear observer

A Passive Non-Linear observer was implemented in order to have access to a 6DOF observer for the system. The algorithms outlined for this observer described in [2] and [12] applied to a 3DOF surface vessel in DP, hence the equations had to be slightly modified in order to be suitable for an ROV. The notation used in Equation 4.9 is explained in Table 2.1.

$$\dot{\hat{\xi}} = A_w + K_1(\omega_0)\tilde{y} \quad (4.9)$$

$$\dot{\hat{\eta}} = J(\eta)\hat{\nu} + K_2\tilde{y} \quad (4.10)$$

$$\dot{\hat{b}} = -T^{-1}\hat{b} + K_3\tilde{y} \quad (4.11)$$

$$M\dot{\hat{\nu}} = -D_L\hat{\nu} - D_{NL}|\hat{\nu}|\hat{\nu} + J^{-1}\hat{b} + \tau + J^{-1}K_4\tilde{y} - C\hat{\nu} \quad (4.12)$$

$$\hat{y} = \hat{\eta} + C_w\hat{\xi} \quad (4.13)$$

In the implementation $y = \eta$ was chosen in order to have full 6DOF system. It is also possible to expand the the observer to include velocity measurements.

The observer gains must be tuned to retain its passivity, and to relate the gains to the dominating wave response frequencies. [12] proposes the following rules for passive observer tuning.

The four gain matrices $\mathbf{K}_1, \mathbf{K}_2, \mathbf{K}_3, \mathbf{K}_4$ are all diagonal:

$$\mathbf{K}_1 = \begin{bmatrix} diag\{k_1, \dots, k_6\} \\ diag\{k_7, \dots, k_{12}\} \end{bmatrix} \quad (4.14)$$

$$\mathbf{K}_2 = diag\{k_{13}, \dots, k_{18}\} \quad (4.15)$$

$$\mathbf{K}_3 = diag\{k_{19}, \dots, k_{24}\} \quad (4.16)$$

$$\mathbf{K}_4 = diag\{k_{25}, \dots, k_{30}\} \quad (4.17)$$

where the values k_1, \dots, k_{30} have the following proposed values:

$$k_i = \begin{cases} -2(\zeta_{ni} - \zeta_i)\frac{\omega_{ci}}{\omega_i} & \text{if } i = 1, \dots, 6 \\ 2\omega_i(\zeta_{ni} - \zeta_i)\frac{\omega_{ci}}{\omega_i} & \text{if } i = 7, \dots, 12 \\ 2\omega_{ci} & \text{if } i = 13, \dots, 18 \end{cases} \quad (4.18)$$

where $\omega_{ci} > \omega_i$ is the filter cut-off frequency. $\zeta_{ci} > \zeta_i$ is a tuning parameter (between 0.5 and 1.0). $k_i, i = 19, \dots, 24$ should be large enough to ensure proper bias estimation. The values $k_i, i = 25, \dots, 30$ have to be tuned according to the final performance of the observer.

$\omega_i = \frac{2\pi}{T_{pi}}$ is the peak response frequency. In most cases, this frequency can be approximated to the peak wave frequency. This is especially true for ROVs, which are much more sensitive to the different wave frequencies than, for example, a ship.

Adaptive observer

In addition to the 4DOF Kalman Filter and the 6DOF Nonlinear Passive Observer, an adaptive observer was implemented into the system. This observer is designed for situations where the parameters of \mathbf{A}_w are not known [28]. This particular feature makes the observer able to adjust wave filter gains to the current sea state through an iterative process, thus making it viable to use in the wave zone for prolonged periods of time. It is uncommon to conduct important missions with an

ROV in the wave zone. However, with the addition of the adaptive observer, it is possible to extend the range of ROV operations closer to the surface.

Adaptive observer design is based on augmented observer equations (equations 4.19 through 4.23) [2].

$$\dot{\hat{\xi}} = \mathbf{A}_w \hat{\xi} + \mathbf{K}_{1h} \tilde{\mathbf{y}}_f \quad (4.19)$$

$$\dot{\hat{\eta}} = \mathbf{J}(\eta) \hat{\nu} + \mathbf{K}_{2l} \tilde{\mathbf{x}}_f + \mathbf{K}_{2h} \tilde{\mathbf{y}}_f \quad (4.20)$$

$$\dot{\hat{b}} = -\mathbf{T}_b^{-1} \hat{b} + \mathbf{K}_{3l} \tilde{\mathbf{y}}_f + \mathbf{K}_{3h} \tilde{\mathbf{y}}_f \quad (4.21)$$

$$\begin{aligned} M \dot{\hat{\nu}} = & -\mathbf{D} \hat{\nu} - \mathbf{J}^\top(\eta) \mathbf{G} \hat{\eta} + \mathbf{J}^{-1}(\eta) \hat{b} + \boldsymbol{\tau} \\ & + \mathbf{J}^{-1}(\eta) (\mathbf{K}_{4l} \tilde{\mathbf{y}}_f + \mathbf{K}_{4h} \tilde{\mathbf{y}}_f) \end{aligned} \quad (4.22)$$

$$\tilde{\mathbf{y}} = \hat{\eta} + \mathbf{C}_w \hat{\xi} \quad (4.23)$$

where $\mathbf{K}_{1h} \in \mathbb{R}^{12 \times 6}$ and $\mathbf{K}_{2l}, \mathbf{K}_{2h}, \mathbf{K}_{3l}, \mathbf{K}_{4l}, \mathbf{K}_{4h} \in \mathbb{R}^{6 \times 6}$ are additional gain matrices to be determined. A new state has been introduced: \mathbf{x}_f , which is the low-pass filtered innovation. It is defined as shown in Equation 4.24 [28].

$$\dot{\mathbf{x}}_f = -\mathbf{T}_f^{-1} \mathbf{x}_f + \tilde{\mathbf{y}} = -\mathbf{T}_f^{-1} \mathbf{x}_f + \tilde{\eta} + \mathbf{C}_w \tilde{\mathbf{i}} \quad (4.24)$$

where $\mathbf{x}_f \in \mathbb{R}^6$, and $\mathbf{T}_f = \text{diag}\{T_{f1}, \dots, T_{f6}\}$ contains filter constants. The high-pass filtered innovation $\tilde{\mathbf{y}}_f$ can be derived from 4.24 in the form of Equation 4.25

$$\tilde{\mathbf{y}}_f = \dot{\mathbf{x}}_f \quad (4.25)$$

The adaptive observer operates with the estimation problem where the parameters of \mathbf{A}_w are unknown [28]. The elements in the matrix vary depending on the current sea-state. Assuming decoupled motions, the composition of the matrix \mathbf{A}_w is shown in Equation 4.26.

$$\mathbf{A}_w(\boldsymbol{\theta}) = \begin{bmatrix} \mathbf{0}_{6 \times 6} & \mathbf{I}_{6 \times 6} \\ -\boldsymbol{\Omega}^2 & -\Delta \boldsymbol{\Omega} \end{bmatrix} \triangleq \begin{bmatrix} \mathbf{0}_{6 \times 6} & \mathbf{I}_{6 \times 6} \\ -\text{diag}(\boldsymbol{\theta}_1) & -\text{diag}(\boldsymbol{\theta}_2) \end{bmatrix} \quad (4.26)$$

where $\boldsymbol{\theta} = [\boldsymbol{\theta}_1^\top, \boldsymbol{\theta}_2^\top]^\top$. The vectors $\boldsymbol{\theta}_1, \boldsymbol{\theta}_2 \in \mathbb{R}^6$ contain the unknown values that are to be estimated. In order for the adaptive law to operate, it is assumed that these values are constant or at least slowly-varying compared to the system states.

Thus, the new WF model is modified as shown:

$$\dot{\hat{\xi}} = \mathbf{A}_w(\hat{\boldsymbol{\theta}}) \hat{\xi} + \mathbf{K}_{1h} \tilde{\mathbf{y}}_f \quad (4.27)$$

The parameter update law for $\boldsymbol{\theta}$ is as follows:

$$\dot{\hat{\boldsymbol{\theta}}} = -\boldsymbol{\Gamma}_w \boldsymbol{\Phi}(\hat{\boldsymbol{\xi}}) \mathbf{C}_h \tilde{\mathbf{x}}_a = -\boldsymbol{\Gamma}_w \boldsymbol{\Phi}(\hat{\boldsymbol{\xi}}) \tilde{\mathbf{y}}_f, \boldsymbol{\Gamma} > 0 \quad (4.28)$$

The regressor matrix $\boldsymbol{\Phi}(\hat{\boldsymbol{\xi}})$ is defined as:

$$\Phi^\top(\hat{\xi}) \triangleq [diag(\hat{\xi}_1) \quad diag(\hat{\xi}_2)] \quad (4.29)$$

The tuning matrices $\mathbf{K}_{1h}, \mathbf{K}_{2l}, \mathbf{K}_{2h}, \mathbf{K}_{3l}, \mathbf{K}_{4l}$ and \mathbf{K}_{4h} should be tuned in a similar manner to the original matrices $\mathbf{K}_1, \mathbf{K}_2, \mathbf{K}_3$ and \mathbf{K}_4 , as described in Section 4.1.1.

The complete structure of the adaptive observer is displayed in Figure 4.1. The structures for the bias and wave estimators, as well as the wave filter, are shown in Figures 4.2, 4.3 and 4.4.

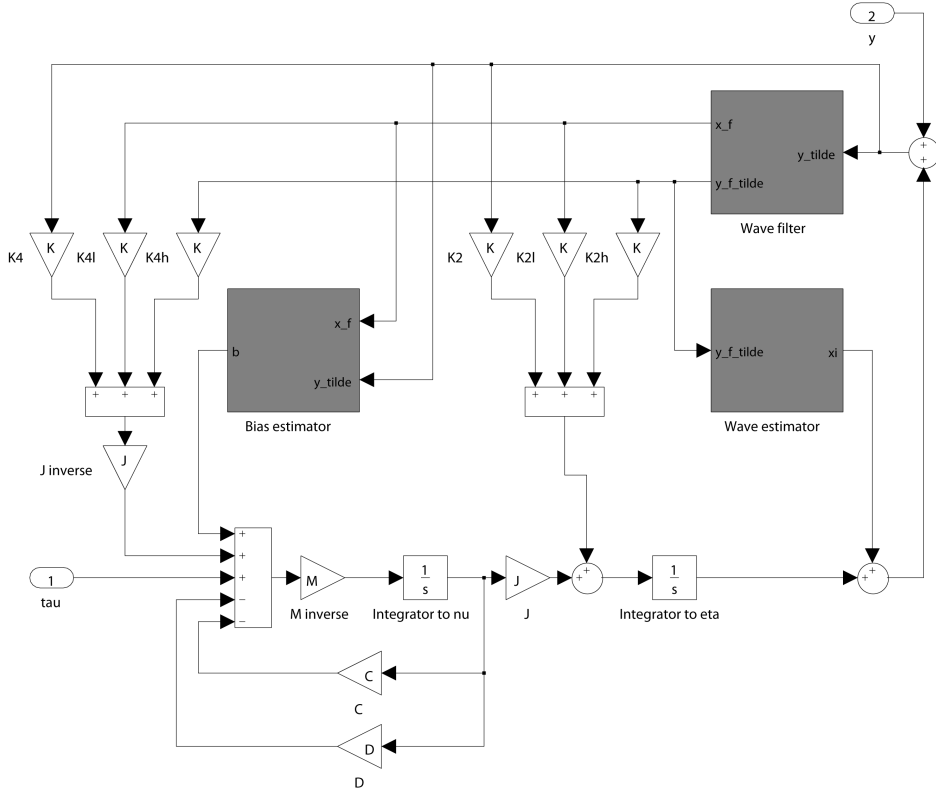


Figure 4.1: Complete model of the adaptive nonlinear passive observer.

4.1.2 Guidance systems

There are two main guidance systems implemented in the system as of June 2012. These are Dynamic Positioning and Joystick mode. The DP guidance system is based on the work done in [29]. Some small modifications in vector and matrix dimension have been done, as well as a new architecture of the method. However, the logic is the same.

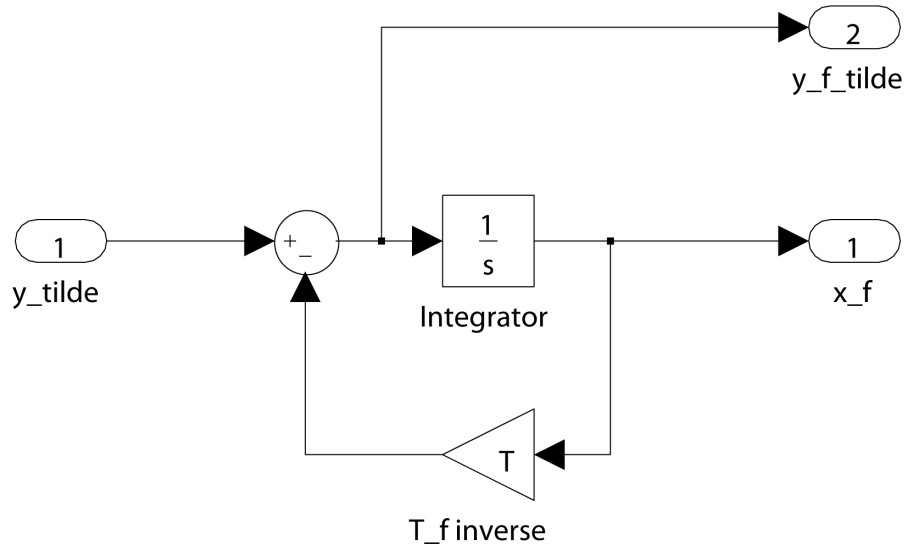


Figure 4.2: Wave filter subsystem including adaptive law.

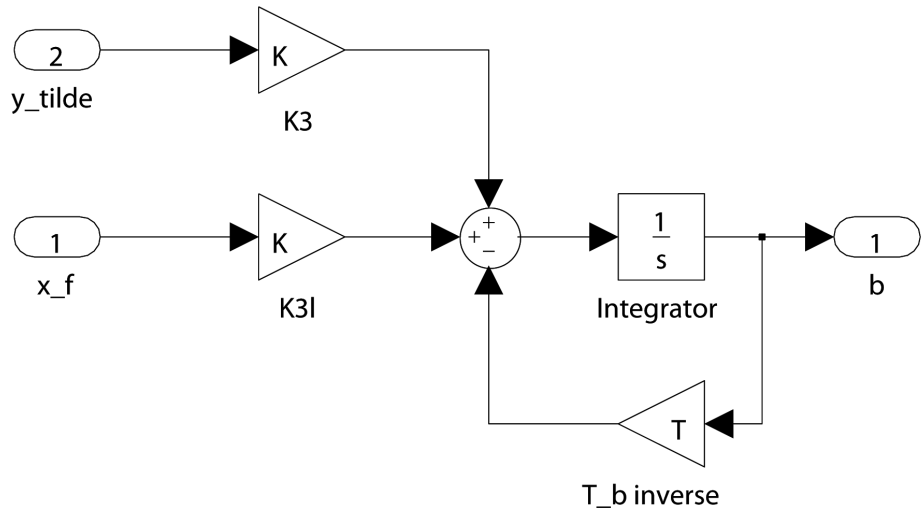


Figure 4.3: Modified bias estimator.

The Joystick mode is based on the work done by Fredrik Dukan in [30]. Some small modifications have been done in the implementation here as well as the

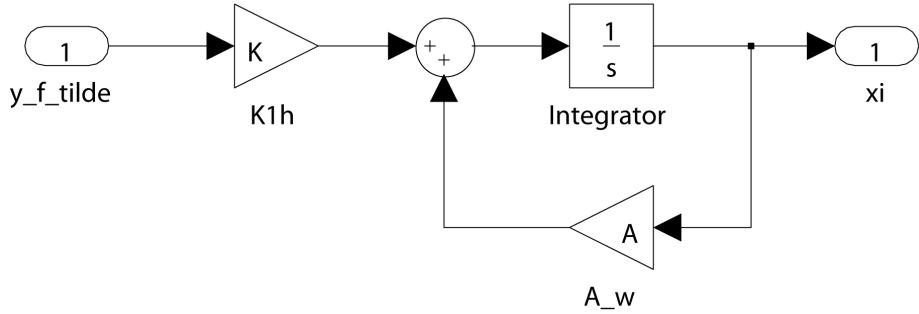


Figure 4.4: Modified wave estimator.

joystick input have been mapped to a number $\in [-100, 100]$ rather than using a bit value $\in [-2^{15}, 2^{15}]$. This mode has three main modes, direct Thrust Allocation, Position Reference, and Velocity Reference. The joystick frame can also be modified between body and NED.

Implementation of a third guidance strategy was attempted. This was a tracking model with a synthetic reference model[31]. However, the complex nature of the guidance strategy created problems during implementation and due to shortage of time, it was abandoned. All guidance systems implemented are set up for 6DOF reference generation. However, only 4 DOFs (Surge/North, Sway/East, Heave/Depth and Yaw/Heading) are given reference values from the user.

4.1.3 Controllers

A selection of controller algorithms was developed for ROV Minerva. When the system was rewritten to accommodate 6 DOFs, the controllers had to be redesigned to be able to control pitch and roll as well as the other 4 DOFs. There are 4 different controllers implemented in the system:

- Linear PID Controller - a very basic control algorithm.
- Non-linear PID Controller - an expansion of the linear PID Controller, including a feedforward term. In the old control system for ROV Minerva, this controller was preferred for full scale tests [16].
- LQR Controller - built on the framework of the non-linear PID controller, but calculates the proportional and derivative controller gain matrices (respectively K_p and K_d) by solving the Riccati equation.
- Sliding Mode Controller - controls the system by forcing it to converge to a stable set of state variables, the so-called *sliding surface*.

The nonlinear PID, LQR, and the Sliding Mode controller are based on the ones described in [16].

Every controller requires adjustments in 2 main areas: integrators and tuning matrices. Due to the way the integrators are implemented, they have to be expanded from 4DOF to 6DOF, most notably the integrator initializing vectors and integrator limits. The tuning matrices also have to be adjusted, in order to accommodate the additional 2 DOFs.

The 6DOF implementation is backwards-flexible. The controllers can now be used for controlling 6DOF systems, while retaining the possibility of controlling systems with a reduced number of DOFs. This is achieved by simply setting the controller gains for the irrelevant DOFs to 0.

4.1.4 Thrust allocation

During the implementation of the thrust allocation algorithm, several alterations to the system were made in order to increase its adaptability in case of thruster failure. The thrust allocation matrix is calculated in real-time during the operation of the system. This allows to make it possible to dynamically alter the matrix in the case of thruster failure. Any thrusters set to be disabled will be excluded during computation of the matrix. In the future, an algorithm to detect any disabled thrusters can be created, which would allow for the operation of the ROV to be automatically adjusted in case of partial failure.

During the calculation of the thrust allocation matrix, a check is performed on the contributions of the thrusters for different DOFs. Since the algorithm is numeric, small rounding errors are present when calculating contributions that are close to 0. In order to avoid unnecessary strain on the ROV motors, errors below 10^{-6} are rounded down to 0.

The control vector \mathbf{u} that comes out of the thrust allocation algorithm is converted to $\mathbf{n}[RPM]$ via Equation 2.45, and is then limited using a saturation function. This function prevents the values in the RPM vector from increasing past the maximum allowed rotational velocity.

4.2 SF 30k telecommunication implementation

The telecommunication buffer, also called telebuf, is the means by which the ROV communicates with the control system. It is set up in such a way as to be able to be interpreted by the local system installed onboard the ROV. This system is what dictates which format the telebuf should operate in. In this case, the telecommunication format was developed by Sperre AS, who developed both ROV Minerva and ROV SF 30k. As a result, the telebufs for the two ROVs are very similar. This significantly simplifies the implementation of the buffer for SF 30k.

In addition, as per request, Sperre AS sent a document with brief descriptions of the telebuf entries. Some of the entries, however, were not properly explained, and thus required further investigation by direct testing. Fredrik Dukan performed this job, and set up a working telebuf for SF 30k, which was then used in the control system.

The telebuf consists of 23 bytes of data, used for transmission of control signals to the thrusters and equipment (cameras and lights). Appendix D shows a detailed breakdown of the telecommunication signals, along with the content of the original email. Since each byte of data can hold any value from 0 to 255, certain bytes are able to control more than one device or setting.

The biggest limitation of using this telebuf system comes when controlling thrusters. Due to the fact that one can only transmit 256 different values means that each thruster can only have 256 speed setpoints. When considering that every thruster is bidirectional, this amount is further reduced to 127 setpoints per direction (as well as one for no thrust, and one leftover). Divided by maximum thruster speed, this would mean that the thrusters can only be controlled in steps of $1500/127 = 11.8\text{RPM}$. However, experiments have shown that the actual resolution is even less, and every thruster only has 64 setpoints in either direction, which results in steps of $1500/64 = 23.4\text{RPM}$.

4.3 SIL and HIL simulator models

In order to be able to test Njord without introducing the risk of equipment damage during sea trials, a simulation environment is required. Two simulation systems are developed for ROV Minerva: a SIL (Software In the Loop) and a HIL (Hardware In the Loop) simulator.

Hardware In the Loop testing technology utilizes the idea of creating a virtual simulation environment that emulates large parts of the system [32]. The main advantage using a HIL simulator lies in the ability to test the functionality of the control system in any kind of failure state, saving large amounts of time and expenses. A HIL simulator is able to detect the following:

- Erroneous configuration parameters
- Design flaws in the software
- Sleeping and hidden software errors
- Missing functionality
- Errors in documentation

In the case of Njord, this simulator can be used to detect any flaws in the design of the system, as well as eliminate most of the implementation errors. It runs on a separate closed-loop system, typically communicating with the system through an interface similar to the interface on the actual ROV. The SIL simulator offers a similar functionality, however it has distinct advantages and disadvantages compared to the HIL version, such as being able to simulate the system at a much faster pace, resulting in shorter simulation time, at the cost of being unable to perform online tuning and adjustments [1].

The basic premise of a HIL simulator is presented in Figure 4.5 (from [33]). The simulator replaces the actual controllable environment with a virtual system

modeled to behave as similar to the real system as possible. The virtual system is able to simulate a wide range of scenarios, including different states of the system, operational and failure modes. This provides an ability to verify the functionality and performance of the control system during normal, abnormal or faulty conditions [34].

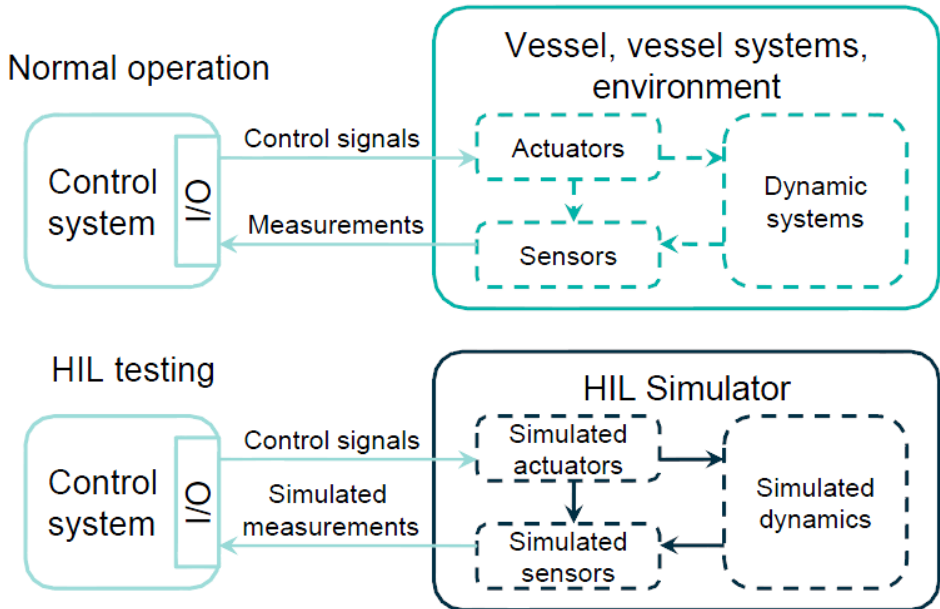


Figure 4.5: The basic concept of hardware-in-the-loop simulation (from [33]).

In order to be able to simulate the ROV, the existing simulator for ROV Minerva has to be reconfigured using the values found in Chapter 2. The following areas of the simulator have to be modified:

- Process plant model
- Thrust dynamics
- Telebuf
- Sensors

During the course of this work, modifications were performed on the first three items in the list. The sensor model remains incomplete, and has to be reconfigured for the changed sensor setup on ROV SF 30k.

Chapter 5

Commissioning and sea trials

A couple of days before the sea trial for the ROV 30k, a series of wet tests were conducted. These were aimed at checking the functionality of original system and ensuring that it worked properly. The vessel's behavior had to be modified such that it had a good balance both in weight-buoyancy ratio and weight distribution. After some weight had been added to the ROV, it seemed more relaxed and easy to control.

The night before the sea trial, the ROV was finally ready to be connected to the new control system. However, during the sea trials, time had to be used on establish full communication between the control system and the ROV. As this was the first time the control system were connected to 30k, there were problems in the sensor setup which had to be fixed before the ROV could be launched in the sea. After the communications were established, the manual thrust control mode was used to check maneuverability given the thruster allocation developed in Section 3.2. The new control system is superior to the original system in this area as the desired thrust is run through thruster allocation. Unwanted movement is then to some degree accounted for, i.e. compensation in pitch angle when going forward.

Due to limited window of operation, tuning of the Kalman Filter was prioritized instead of the Nonlinear PID controller, as it was a necessity in order to be able to try the DP system. After reducing the response of the estimated surge and sway velocities, \hat{u} and \hat{v} , the observer behaved in accordance with the measured values. The bias component had to be tuned as well, as there were stationary deviations in the North and East position estimates.

Figure 5.1 shows the position data for 30k during DP operation. From 10 to about 90 seconds the ROV performed station keeping at its position at the activation time for DP Mode, $\boldsymbol{\eta}_{ref} = [0, 0, 33.5, 2.2, 1.8, -50]^\top$. Even though the Nonlinear PID controller was not tuned, it managed to keep the ROV on position. The lack of controller tuning can especially be seen in the transit between two set points. After about 90 seconds a new position was given to the ROV, $\boldsymbol{\eta}_{ref} = [2, 0, 33.5, 0, 0, 0]^\top$. The first graph in Figure 5.1 indicates that the proportional gain is too low. This is in accordance with the fact that the tuning values used are exactly the same as for Minerva, which is a much smaller and more agile ROV. The

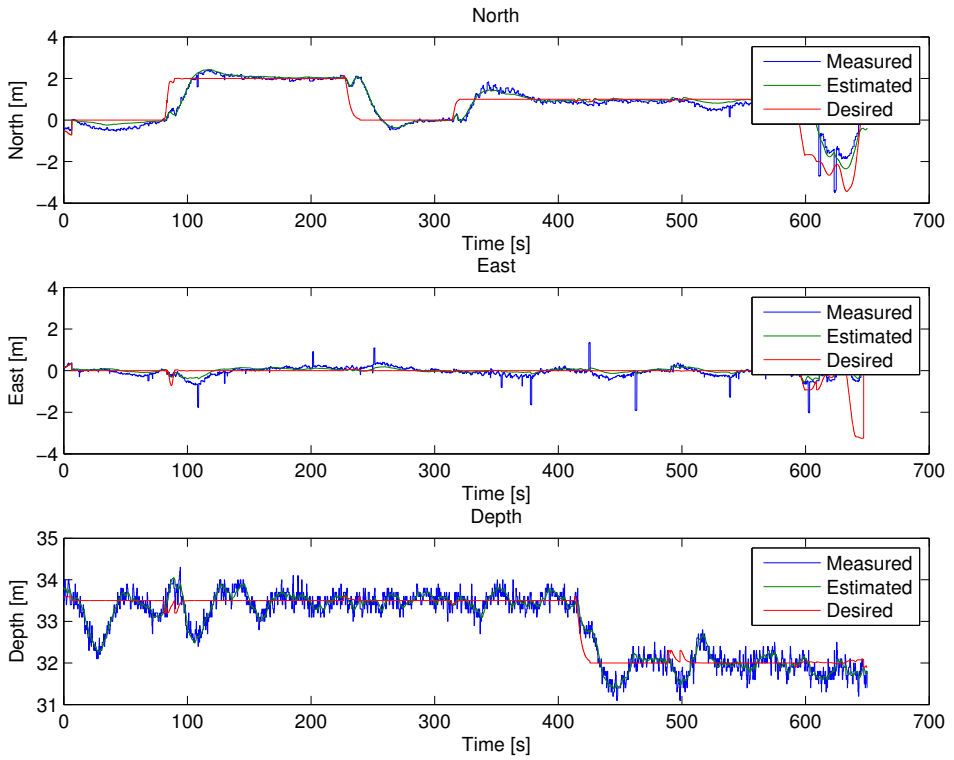


Figure 5.1: Plots of Translational motion during DP test.

reference model parameters in the guidance system were also suited for Minerva rather than 30k, which can be seen by the rapid increase in desired position.

The orientation of the ROV during DP operation is shown in Figure 5.2. Graph number three is of most interest as it illustrates the heading angle of . It can be seen that the controller makes the ROV follow the reference. However, the same problem as described above yield in yaw as the controller is too weak to reduce the error in a timely manner. The orientations of the ROV is measured with a Xsense MTi [35], which is a gyro-enhanced Attitude and Heading Reference System (AHRS). This sensor has its own observer and is more accurate than the compass measurements from the DVL. The estimated attitude values are sent to the Kalman Filter in order to estimate the yaw rate, $\dot{\gamma}$, as well as being used in the estimated position vector, $\hat{\eta}$. Because of this the plot of the measured heading values is hidden behind the estimated values.

In Figure 5.2, the first station keeping period (10-90 seconds) has desired values in accordance to the logic mentioned above, i.e. station keeping of position at activation time for DP Mode. When a new reference position is given, a fault occurs in the desired roll value. This should have been set to zero. However, as both roll and pitch are not independently controlled due to the ROV thruster

configuration, the fault never propagates and becomes a failure.

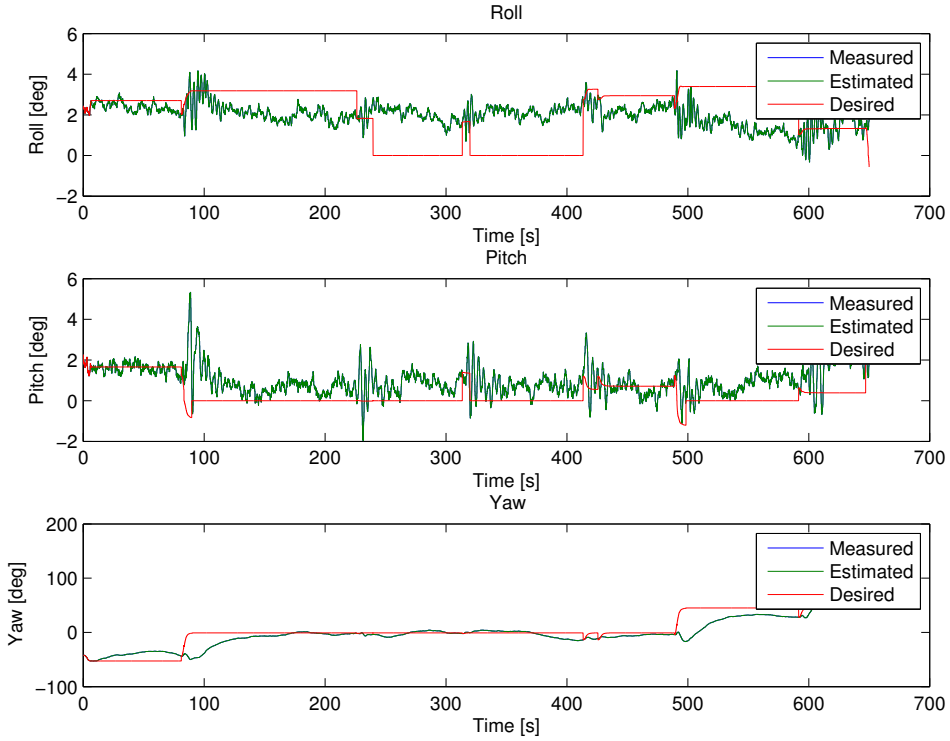


Figure 5.2: Plots of Rotational motion during DP test.

After about 680 seconds in Figure 5.1 and 5.2, or 50 seconds in Figure 5.3 and 5.4 manual thrust control with joystick was activated. These plots indicate that the observer manages to follow the measurements in a satisfactory manner, hence the Kalman Filter is working properly.

In Joystick Mode with Force control frame, the desired position values are set to the estimated values, $\eta_d = \hat{\eta}$. This results in a plot with only one graph for yaw angles as measured, estimated and desired values are the same.

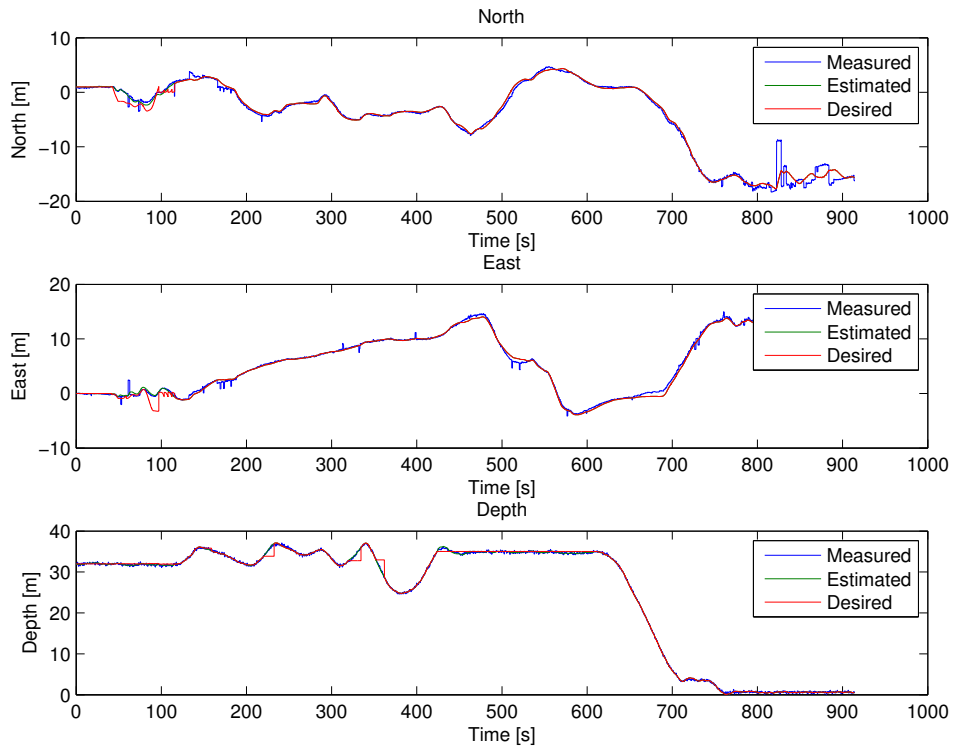


Figure 5.3: Plots of Translational motion during Direct Thrust Allocation Mode with Joystick.

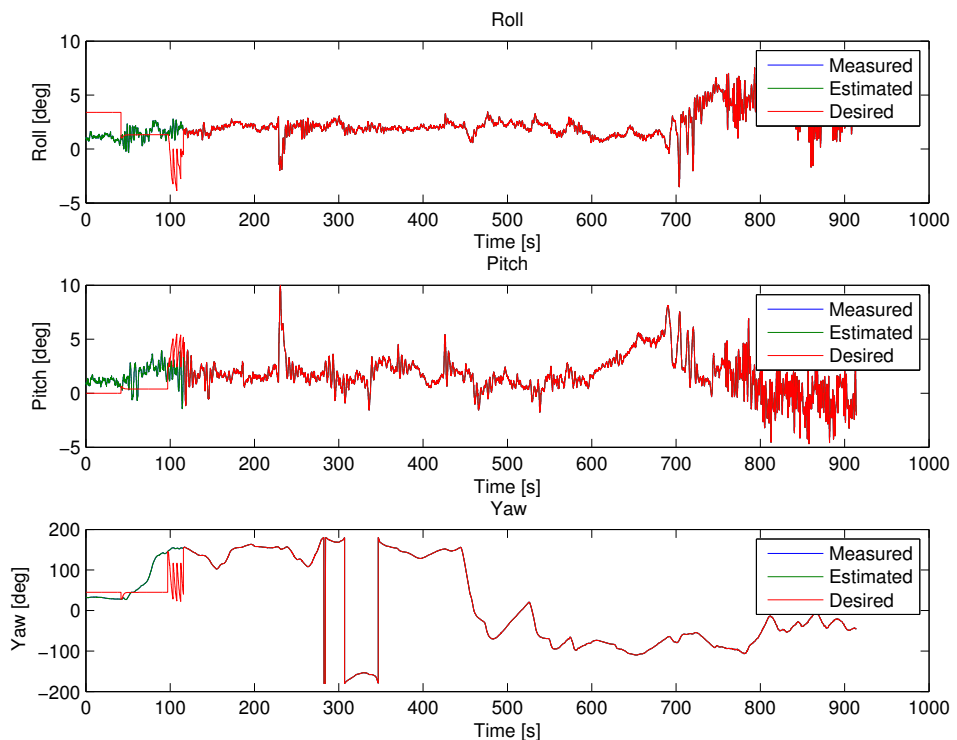


Figure 5.4: Plots of Rotational motion during Direct Thrust Allocation Mode with Joystick.

Chapter 6

Conclusions and further work

6.1 Conclusions

The prime goal of this thesis was the commissioning of a DP control system for ROV SF 30k. A large amount of work has been done within this thesis in order to achieve that.

The primary focus was the establishment and estimation of the mathematical model of the ROV. The parameters of the model were not always possible to find analytically or empirically, and thus a number of assumptions were made. A 3D model of the vessel was provided by Sperre AS. It was simplified using a variety of 3D modeling programs and then was used as a basis for calculation of rigid body and added mass kinetics of the ROV. No data representing the damping parameters of the ROV is present, which made it necessary to estimate the values based on other methods. Since ROV Minerva and ROV SF 30k have rather similar shapes and proportions, the damping coefficients for SF 30k were guesstimated based on those found for Minerva.

In order to set up a thrust allocation system, thrust dynamics were determined based on the 3D model, as well as thruster properties, which were also provided by Sperre AS. The thrust allocation was implemented into the DP system, and later tested in the sea trials. During manual operation of the ROV, the thrust allocation system was used to provide direct thrust control, which has shown that the thrust configuration matrix was set up properly. The system was able to allocate thrust commanded by the joystick to the actuators on the ROV, ensuring that any coupled motions (such as the fact that the tunnel thruster produces a yaw moment) were accounted for.

The thrust coefficient matrix was found based on curve regression from Appendix C. During this thesis, the curve for thrusters SE120/150 was regressed. However, during sea trials, the second curve (for thrusters SE80/100) was regressed and tested as well. However, it proved to not provide sufficient thrust, and thus

the system was reverted back to using the coefficients from the SE120/150 curve.

The model was implemented into the DP system developed by Espen Tolpinrud [1]. Additionally, the author of this thesis contributed to porting several modules from the old DP system, which was tailor-made for ROV Minerva, into the more generalized new one. This includes the porting and modification for 6DOF of all controllers (linear and nonlinear PID, LQR, Sliding Mode), the Kalman Filter and the thrust allocation module. An effort was made to make these modules as general as possible, with the future purpose of being able to use them on any arbitrarily defined ROV.

As an addition to the passive nonlinear 6DOF observer developed by Espen Tolpinrud, an adaptive observer was designed and partially implemented into the system. Due to the fact that the ROV was not required to operate in the wave-zone, it was not completed. It can, however, be developed to be used in the future for operating the ROV close to the surface, which is beneficial for shallow water or offshore operations.

The sea trials for ROV SF 30k had a small window of operation. The reason for this is the fact that the DP control system did not have the necessary functionality to be used on an ROV. When the system gained enough functionality, a large amount of work was required to prepare the ROV for sea trials. Because of this, the DP system was not completely adjusted to work with the ROV before the start of the cruise that was scheduled for testing it.

When testing the ROV in DP mode, the Kalman Filter was used, as it was extensively tested previous to being ported to the new DP system, and was thus faster to adapt for SF 30k. Tests have shown that the observer was abnormally fast when compared to the real system. Two possible solutions were available: tuning down the thrust coefficients, or increasing the mass of the vessel in the observer. Since modifying thrust allocation affected the behavior of the ROV adversely, it was decided to scale up the mass of the vessel. Due to time constraints, the source of the error was not determined, however, it might be attributed to an error in modelling.

6.2 Recommendations for further work

Preliminary testing of the control system at the sea trials showed that the model derived within this thesis is reasonably accurate. However, certain parameters have to be analyzed more accurately in order to improve the efficiency of the observers and controllers.

Damping coefficients are the primary area for further improvement, as most of the values were roughly guesstimated. Ideally, a series of towing tests could be performed on a scaled model of SF 30k. These tests were not within the scope of this thesis, and thus the values were roughly approximated based on ROV Minerva. While such an approach might provide a sufficient accuracy for the control system, which can compensate for eventual modelling errors by control dynamics, a more precise model is necessary in order to complete the SIL and HIL simulators.

In regards to the simulators, the signal modeling part needs to be fitted for SF

30k, most notably the sensor offsets, which are different between ROV Minerva (which the simulators use) and ROV SF 30k.

As of June 2012, the control system can not operate within the wave zone. This is attributed to two shortcomings: an incomplete wave estimator within the observers, and lack of hydrodynamic data for the ROV. It is recommended to perform a series of WAMIT simulations in different depths and sea states in order to determine the added mass coefficients within different conditions. Furthermore, the wave estimator has to be completed. The main focus of improvement within it is design of a proper significant wave frequency predictor. The adaptive observer also has to be tuned appropriately. It has the basic functionality, but does not produce proper estimated values.

Bibliography

- [1] E. Tolpinrud. Implementation of computer-based control systems for rovs. Master's thesis, Norwegian University of Science and Technology, 2012.
- [2] T.I. Fossen. *Handbook of Marine Craft Hydrodynamics and Motion Control*. Wiley, 2011.
- [3] G. Tierie. *Cornelis Drebbel*. Amsterdam: HJ Paris, 1932.
- [4] F. Wagner. *Submarine fighter of the American Revolution: the story of David Bushnell*. Dodd, Mead, 1963.
- [5] D.R. Blidberg. The development of autonomous underwater vehicles (auvs); a brief summary. In *IEEE ICRA*, volume 6500, 2001.
- [6] C. von Alt. Autonomous underwater vehicles. In *Autonomous Underwater Lagrangian Platforms and Sensors Workshop*, 2003.
- [7] Wikipedia. Remotely operated underwater vehicle. http://en.wikipedia.org/wiki/Remotely_operated_underwater_vehicle, 2012. [visited 04.06.2012].
- [8] NTNU. Aur lab. <http://www.ntnu.edu/news/aur-lab>, 2011. [visited 02.06.2012].
- [9] Svenn Ole Linde. Pictures of minerva. <http://www.ntnu.edu/marine/minerva/pictures>, 2012. [visited 06.06.2012].
- [10] Kraft Telerobotics. Raptor remotely operated force feedback manipulator arm system. <http://krafttelerobotics.com/products/raptor.htm>, 2012. [visited 03.06.2012].
- [11] N. Minorsky. Steering of ships. 1984.
- [12] A.J. Sørensen. *Marine Control Systems. Propulsion and motion control of ships and ocean structures*. Norwegian University of Science and Technology, 2011.
- [13] T.I. Fossen. *Nonlinear modelling and control of underwater vehicles*. PhD thesis, Norwegian University of Science and Technology, 1991.

- [14] *Nomenclature for treating the motion of a submerged body through a fluid: report of the American Towing Tank Conference.* Technical and research bulletin. Society of Naval Architects and Marine Engineers, 1950.
- [15] T.I. Fossen and O.E. Fjellstad. Nonlinear modelling of marine vehicles in 6 degrees of freedom. *Mathematical Modelling of Systems*, 1(1):17–27, 1995.
- [16] M. Kirkeby. Comparison of controllers for dynamic positioning and tracking of rov minerva. Master's thesis, Norwegian University of Science and Technology, 2010.
- [17] O.M. Faltinsen. *Sea loads on ships and offshore structures.* Cambridge University Press, 1990.
- [18] B. Sortland and K. Vartdal. Optimization of rov pipeline inspection speed. In *On the shores of tomorrow: Intervention'90 Conference and Exposition, June 25-27, 1990, Vancouver Trade & Convention Centre, Vancouver, British Columbia, Canada*, page 118. Marine Technology Society, 1990.
- [19] J. Carlton. *Marine Propellers and Propulsion.* Elsveier Ltd., 2007.
- [20] S.L. Campbell and C.D. Meyer. *Generalized Inverses of Linear Transformations.* Classics in Applied Mathematics. Society for Industrial and Applied Mathematics, 2009.
- [21] INC. WAMIT. Wamit user manual. <http://www.wamit.com/manual.pdf>, 2011.
- [22] Norwegian University of Science and Technology. Ntnu, minerva specifications. <http://www.ntnu.edu/marine/minerva/specifications>, 2003.
- [23] S. Steen. *Motstand og propulsjon - propell- og foilteori.* Norwegian University of Science and Technology, 2007.
- [24] E. Svendby. Robust control of rov/auvs. Master's thesis, Norwegian University of Science and Technology, 2007.
- [25] Intel Corporation. Intel processor specifications. <http://www.intel.com/content/www/us/en/processor-comparison/processor-specifications.html?proc=43122>, 2009. [visited 18.05.2012].
- [26] National Instruments. Using local and global variables carefully. http://zone.ni.com/reference/en-XX/help/371361E-01/lvconcepts/using_local_and_global/, 2008. [visited 18.05.2012].
- [27] National Instruments. Are labview global variables good or bad, and when is it ok to use them? <http://zone.ni.com/devzone/cda/tut/p/id/5317>, 2011. [visited 13.12.2011].

- [28] Jann Strand and Thor Fossen. Nonlinear passive observer design for ships with adaptive wave filtering. In H. Nijmeijer and T.I. Fossen, editors, *New Directions in nonlinear observer design*, volume 244 of *Lecture Notes in Control and Information Sciences*, pages 113–134. Springer Berlin / Heidelberg, 1999. 10.1007/BFb0109924.
- [29] S.Ø. Kørte. Guidance & control strategies for uuv's. Master's thesis, Norwegian University of Science and Technology, 2011.
- [30] F. Dukan and A. J. Sørensen. Joystick in closed-loop control of rovs with experimental results. Technical report, Norwegian University of Science and Technology, Department of Marine Technology and Centre for Ships and Ocean Structures, 2012.
- [31] D. A Fernandes, F. Dukan, and A. Sørensen. Reference model for higher performance and lower energy consumption in motions of marine crafts: Theory and experiments. *IEEE Journal of Oceanic Engineering*, 2011.
- [32] T.A. Johansen and A.J. Sørensen. Experiences with hil simulator testing of power management systems. *Marine Technology Society, Houston, US*, 2009.
- [33] Ø. Smogeli. Third party hil testing of control system software. Marine Cybernetics, 2011.
- [34] Ø. Smogeli. Experiences from five years of dp software testing. Marine Cybernetics, 2010.
- [35] Xsense. Mti. <http://www.xsens.com/en/general/mti>, 2012. [visited 01.06.2012].

Appendix A

ROV 30k specifications



SUB-fighter 30K

Heavy duty electric work-class ROV
Dynamic Positioning, DP available
Industry and science applications
Interface for standard tools
Additional tools on skid
Control container
Reliable and well proven design

STANDARD SPECIFICATION SUB-fighter 30K

Standard delivery:

Vehicle LWH 250 x 150 x 160 cm.

Frame: Aluminum, black anodized

Housings: 2 electronic pressure bottles

Weight in air: Approximately 1350 kg

LARS: 1,5 ton latch with auto release

Payload : 60 kg.

Max. depth: 700 m.

Power input: 230 VAC, 3 phase, 30 kW.

Thrusters: 6 thrusters with 3kW,
pressure compensated,

Speed app.: Horizontal 2.1 knot
Vertical 1.8 knot
Lateral 0,9 knot
Turn 90 deg/sec.

Manipulator: Hydraulic or electric available



Lights: 4 x 250W halogen lights
4 channel light dimmer

Camera: 7 camera interfaces
PAL color CCDs
Color camera 0.1 lux
Zoom camera, Sony
SIT camera
HD-SDI camera

Telemetry: Fiber optic CWDM system
Focal mux, model 907
4 video, synchronous
16 RS 232 channels
5 RS 485 channels
3 port 20 base Ethernet

Sensors: Depth sensor, accurate 0.15%
Fluxgate compass,
Leakage detector

Auto func.: DP, Dynamic positioning
AD, Auto depth
AH, Auto heading



Notodden Næringspark
Postboks 44
N-3671 Notodden
Norway

OPTIONS ROV

Depth

700 - 3000 meter depth rating

LARS and TMS

Different models

Manipulators and HPU

Different hydraulic manipulators

7-5-4-3 function

Standard electric grabber manipulator

Hydraulic cable cutter

HPU 5,5 kw. 18 l/min. 140 bar

Video and Still cameras

Mini color camera

LL CCD monochrome camera

Zoom camera

3 CCD zoom camera HD-

SDI camera Stillcamera, 8

mPix. Online Photo mosaic
camera

Light

Halogen lights, 250 W

HMI gas lights, 200 and 400 W

Auto functions

DP, Dynamic Positioning system

AA, Auto altitude

ATC, Auto track control – closed loop control
(if integrated LBL system and doppler/MRU)

Position and survey system

SSBL HPR system

LBL, integrated into ROV

EIVA survey mapping and monitoring
system

Other sensors and equipment

Scanning sonars

Multibeam

Cable tracker

Side scan

Altimeter

Doppler log

MRU

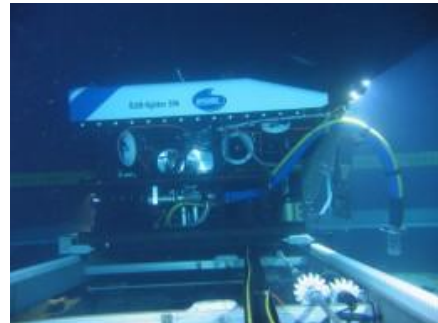
Lasers

HPR LBL integrated

Transponders

1 kw. Vacuum pump

2,2 kw. Water pump





Notodden Næringspark
Postboks 44
N-3671 Notodden
Norway

Control container



Video storing: DVD standard, HDD (option)



Size: Std ISO, 20' container. AC system

Weight: 2800 kg

Power input: 230 VAC , 3 phase, 30 kW.

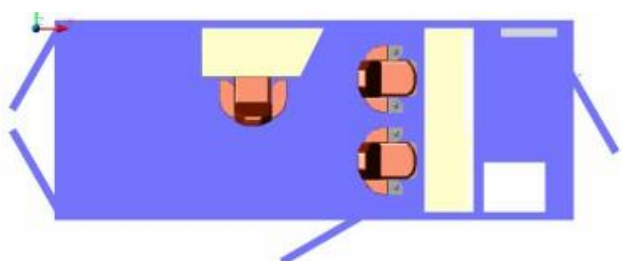
Pilot chairs: 2 leather chairs

Rack: ROV system PC,
Video switch and quad
Focal multiplexer

ROV Control: ROV control, integrated in chair. Mobile ROV control for outside use

Viewing: 42" Plasma videomonitor,
5 LCD screens for data

Overlay: Vig Option
overlay, screenwriter and
video grabber





Notodden Næringspark
Postboks 44
N-3671 Notodden
Norway

Umbilical storage winch



Winch with 2000 m cable

Cable speed

Layer 1 : 0 – 20.4 m/min.
Layer 9 : 0 - 34.5 m/min.

Electric input

Single phase 230 V AC 50 Hz. 16 A

Controls

Manual control with 10 meters cable.
Emergency stop, up, down and speed control.

Slip ring

Focal electro/optical model 176/190

Brake

Automatic self blocking gearbox

Storage winch for ROV tether

Overall dimensions

Width	2500 mm.
Height	1550 mm.
Depth	1450 mm.

Drum dimension

Core length	1500 mm.
Core diameter	610 mm.
Flange diameter	1050 mm.

Cable capacity

1100 meter of 27 mm. cable diameter

Weight

Approx 1350 kg. with cable

Cable pull, theoretic

Layer 1	3942 N
Layer 9	2464 N

Appendix B

Model files

B.A Original model

Located in folder “Appendices/Appendix B/Appendix B-A”.

B.B Simplified model

Located in folder “Appendices/Appendix B/Appendix B-B”.

B.C Converted model

Located in folder “Appendices/Appendix B/Appendix B-C”.

B.D WAMIT model

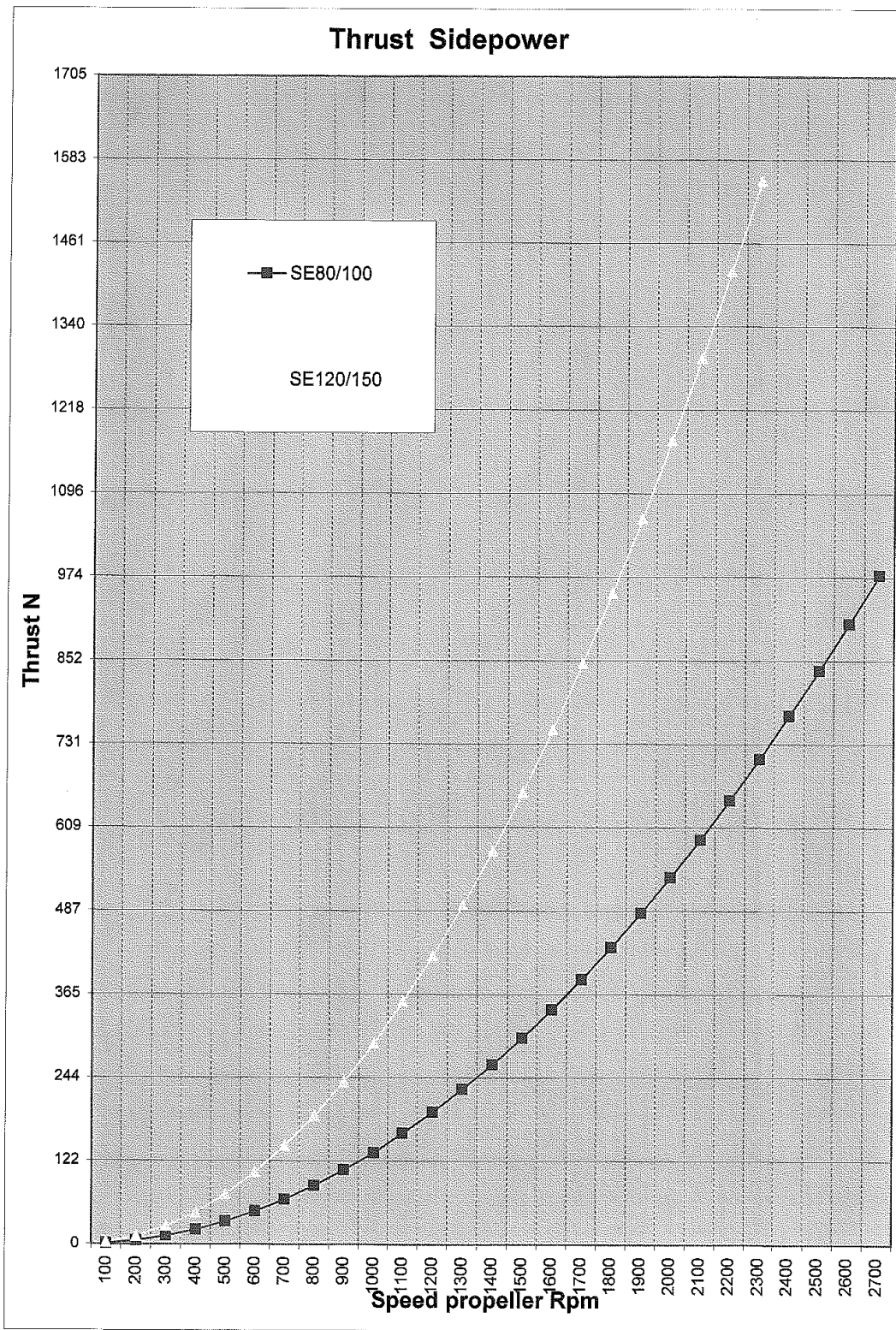
Located in folder “Appendices/Appendix B/Appendix B-D”.

B.E Model used to calculate projected area

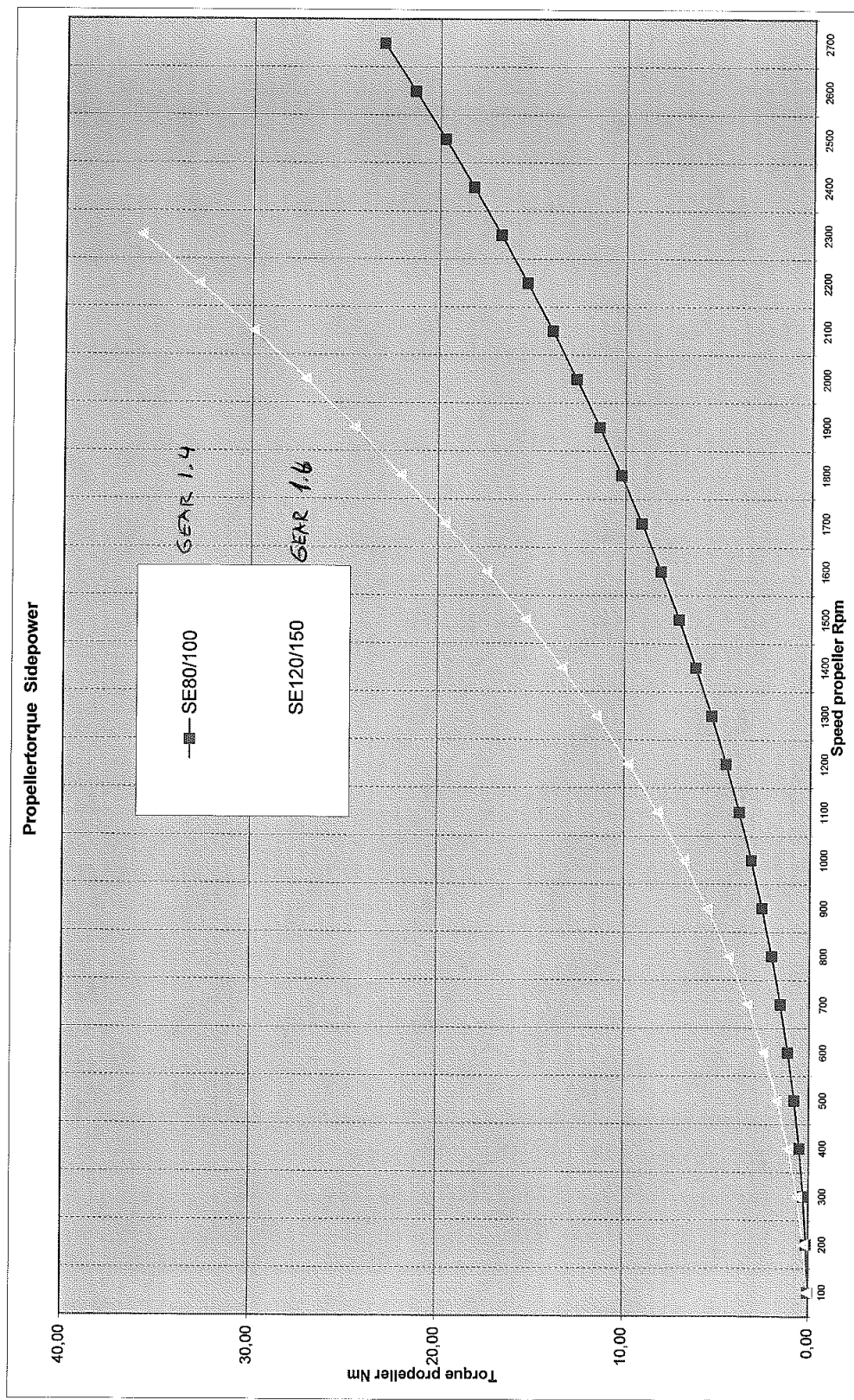
Located in folder “Appendices/Appendix B/Appendix B-E”.

Appendix C

RPM-to-thrust data



ORIGINAL



Appendix D

Information on the telecommunication buffer for ROV SF 30k

Telebuf protocol for Sperre 30k ROV

```
/* Dataformat:  
 * RS232  
 * 9600,n,8,1  
 */  
  
/*  
 * the receive-data-from-surface process  
 *  
 * data are received on the B-port of QUART  
 *  
 * telegram format (26 bytes) :  
 * 7 bits for data, bit 8 (0x80(hex80)) is startbit.  
  
 * 00: start (0x9C) (startbit + telegram length)  
 * 01: forward (forward thrust)  
 * 02: turn (jalla thruster allocation)  
 * 03: z1 (chair right joystick turn, not in use in org. setup)  
 * 04: vertical (all vertical thrusters)  
 * 05: side (side thrusters)  
 * 06: z2 (chair left joystick turn, not in use in org. setup)  
 * 07: MSB thruster (Most significant bit of thrusters)  
 * 08: thrust (knob for vertical thrust)  
 * 09: dimmer 1 (dimmer for lights 1)  
 * 10: dimmer 2 (dimmer for lights 2)  
 * 11: dimmer 3+4 (dimmer for lights 3+4)  
 * 12: spare 1 (spare knob on control panel)  
 * 13: spare 2 (vacuum pump knob)  
 * 14: extra thruster (excavation unit knob)  
 * 15: digital 1 (switch remote/chair joystick, trim, power excavation unit)  
 * 16: digital 2 (lights 1-4, tilt/pan)  
 * 17: digital 3 (Kraft power, HMI 1-2, HPR)  
 * 18: digital 4 (Sonar 1-2, Doppler, laser, pan/tilt, transponder, still cam)  
 * 19: digital 5 (vacuum pump, wet mate)  
 * 20: digital 6 (zoom 1-2,camera selector 1-4)  
 * 21: digital 7 (pressure -/+ , vacuum -/+ , collect unit out/in, ccw)  
 * 22: digital 8 (lock, test, to/from)  
 * 23: MSB digital (Most significant byte: HD cam, cam 2, sss, collect unit cw, tilt up)  
 * 24: AF digital (Auto depth/heading)  
 * 25: checksum 1  
 * 26: checksum 2
```




Figure 1: 30k Control panel



Figure 2: 30k portable command console



Figure 3: Joystick on chair

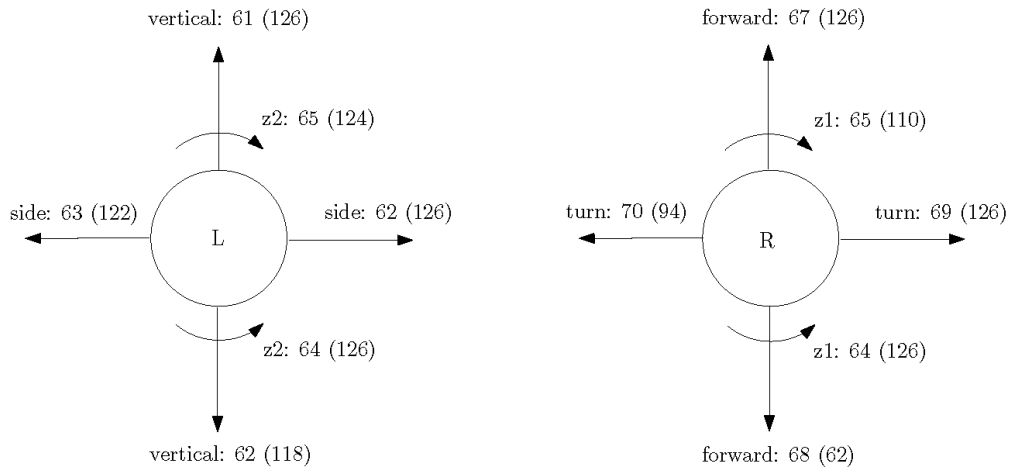


Figure 4: Maximum byte value of joysticks in chair; max byte value (MSB thruster)

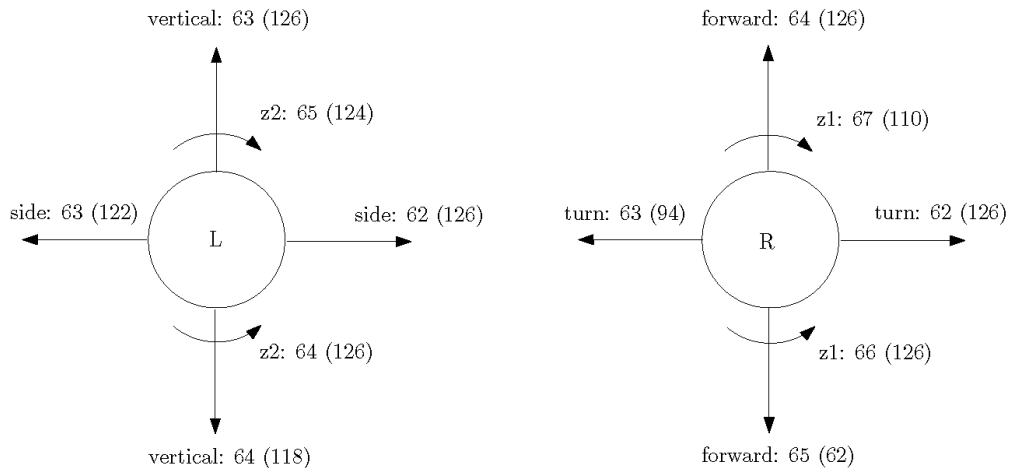


Figure 5: Maximum byte value of joysticks on portable command console; max byte value (MSB thruster)